Journal of Applied Physics

RESEARCH ARTICLE | OCTOBER 06 2025

Phonon Olympics: Phonon property and lattice thermal conductivity benchmarking from open-source packages

Alan J. H. McGaughey ; Lucas Lindsay ; Hua Bao ; Tomu Hamakawa ; Rinkle Juneja ; Shouhang Li ; Wu Li ; Ryota Masuki; Fanchen Meng ; Han Meng; Tribhuwan Pandey ; Cheng Shao ; Junichiro Shiomi ; Terumasa Tadano ; Atsushi Togo ; Ao Wang ; Xinyu Zhang

J. Appl. Phys. 138, 135108 (2025)
https://doi.org/10.1063/5.0289819
CHORUS

AIP Publishing

Journal of Applied Physics ARTICLE pubs.aip.org/aip/jap

Phonon Olympics: Phonon property and lattice thermal conductivity benchmarking from open-source packages

Cite as: J. Appl. Phys. **138**, 135108 (2025); doi: 10.1063/5.0289819
Submitted: 9 July 2025 · Accepted: 17 September 2025 ·
Published Online: 6 October 2025

Alan J. H. McGaughey,[1,a)] Lucas Lindsay,[2,b)] Hua Bao,[3] Tomu Hamakawa,[4,5] Rinkle Juneja,[2] Shouhang Li,[6] Wu Li,[7,8] Ryota Masuki,[9] Fanchen Meng,[10] Han Meng,[4,11] Tribhuwan Pandey,[12] Cheng Shao,[4,13] Junichiro Shiomi,[4,11] Terumasa Tadano,[14,15] Atsushi Togo,[16] Ao Wang,[3] and Xinyu Zhang[3]

AFFILIATIONS

[1]Department of Mechanical Engineering, Carnegie Mellon University, Pittsburgh, Pennsylvania 15213, USA
[2]Materials Science and Technology Division, Oak Ridge National Laboratory, Oak Ridge, Tennessee 37831, USA
[3]Global Institute of Future Technology, Shanghai Jiao Tong University, Shanghai 200240, China
[4]Department of Mechanical Engineering, The University of Tokyo, 7-3-1 Hongo, Bunkyo, Tokyo 113-8656, Japan
[5]Research Organization of Information and Systems, The Institute of Statistical Mathematics, Tachikawa, Tokyo, Japan
[6]College of Mechanical Engineering, Donghua University, Shanghai 201620, China
[7]Eastern Institute for Advanced Study, Eastern Institute of Technology, Ningbo 315200, China
[8]Institute for Advanced Study, Shenzhen University, Shenzhen 518060, China
[9]Department of Applied Physics, The University of Tokyo, 7-3-1 Hongo, Bunkyo-ku, Tokyo 113-8656, Japan
[10]Watt Family Innovation Center, Clemson, South Carolina 29634, USA
[11]Institute of Engineering Innovation, The University of Tokyo, 7-3-1 Hongo, Bunkyo, Tokyo 113-8656, Japan
[12]Department of Physics, University of Antwerp, Groenenborgerlaan 171, Antwerp B-2020, Belgium
[13]Thermal Science Research Center, Shandong Institute of Advanced Technology, Jinan, Shandong Province 250103, China
[14]Research Center for Magnetic and Spintronic Materials, National Institute for Materials Science, Tsukuba, Ibaraki 305-0047, Japan
[15]Digital Transformation Initiative Center for Magnetic Materials, National Institute for Materials Science, Tsukuba, Ibaraki 305-0047, Japan
[16]Center for Basic Research on Materials, National Institute for Materials Science, Tsukuba, Ibaraki 305-0047, Japan

[a)]**Author to whom correspondence should be addressed:** mcgaughey@cmu.edu
[b)]**Electronic mail:** lindsaylr@ornl.gov

ABSTRACT

Three widely used open-source packages for determining phonon properties and lattice thermal conductivities (ALAMODE, phono3py, and ShengBTE) are benchmarked by teams of expert users and the package developers. The phonons for Ge, RbBr, monolayer $MoSe_2$, and AlN are modeled at zero temperature, and they scatter through three-phonon and phonon-isotope processes, with thermal conductivities obtained from the linearized Peierls–Boltzmann transport equation with input from density functional theory calculations. Over a wide range of temperatures, the thermal conductivities calculated by the teams fall within at most $\pm 15\%$ of their mean values for each of the four materials. The phonon frequencies, obtained from the harmonic force constants, do not show large differences between the calculations, indicating that the modal heat capacities and group velocities are not responsible for the thermal conductivity variations. It is the lifetimes associated with three-phonon scattering, obtained from the cubic force constants, that drive the variations. The many decisions required to calculate the cubic force constants (e.g., supercell size, atomic displacement, neighbor cutoff, and application of symmetries)

make identification of the precise origin of the thermal conductivity variations challenging. The calculated thermal conductivities do not generally show agreement with experimental measurements, which is attributed to the limitations of the density functional theory calculations. Guidance for the development of best practices is provided, which will help to standardize protocols needed for building thermal conductivity databases. The results provide a baseline for future benchmarking of other packages and more advanced calculations.

 https://doi.org/10.1063/5.0289819

I. INTRODUCTION

The integration of density functional theory (DFT) calculations, lattice dynamics theory, and solutions to the linearized Peierls–Boltzmann transport equation (PBTE) have enabled first-principles-driven predictions of phonon properties and lattice thermal conductivities that agree with experimental measurements for a range of materials.[1–4] While open-source and commercial DFT packages have long been available, early phonon property and thermal conductivity calculations were performed using in-house codes for the lattice dynamics and PBTE. Over the last decade, open-source packages have been released for performing these calculations,[5–17] enabling the broad research community to study thermal transport by phonons. While each package has a similar workflow, differences exist in how they are used by researchers and in how the underlying algorithms are implemented, which may impact calculations.

As established researchers transition from in-house codes to open-source packages, as new researchers enter the field using these packages, and as new computational capabilities are implemented based on the foundation provided by these packages, there is a growing need to assess their performance. The objective of this study is to benchmark three commonly used open-source packages (ALAMODE,[5] phono3py,[6,7] and ShengBTE[8]). One package will not be identified as being better than the others. Instead, how the developers and expert users apply these packages to a set of materials that span different compositions, crystal structures, bonding environments, and thermal conductivity magnitudes will be presented. The results will be used to suggest best practices for calculating phonon properties and thermal conductivity. The establishment of such best practices is essential for building databases[18–20] and for enabling repeatability and validation of published results.

This paper is organized as follows. The procedure for calculating phonon properties and thermal conductivity is briefly summarized in Sec. II, and the studied materials are described in Sec. III. The benchmark process is explained in Sec. IV, with details about the packages, the teams, and the calculation chronology. The results are presented in Secs. V and VI, with a focus on dispersion curves, temperature-dependent thermal conductivities, frequency-dependent thermal conductivity accumulation functions, and lifetimes. The results are discussed in the context of experimental measurements in Sec. VII, suggested best practices are provided in Sec. VIII, and the paper concludes with a summary and outlook in Sec. IX.

II. LATTICE THERMAL CONDUCTIVITY CALCULATION

The workflow for calculating lattice thermal conductivity is described in previous reports.[4,8,9,21] A short summary is provided here. The ultimate objective is to evaluate the thermal conductivity in the α-direction, k_α, from

$$k_\alpha = \sum_i c_i v_{g,\alpha,i}^2 \tau_{\alpha,i}. \quad (1)$$

The summation is over the phonon modes in the first Brillouin zone. c_i, $v_{g,\alpha,i}$, and $\tau_{\alpha,i}$ are the mode-dependent volumetric heat capacity, the α-component of the group velocity vector, and the α-direction lifetime. This benchmarking project is limited to phonons obtained from zero-temperature DFT theory that scatter through three-phonon and phonon-isotope processes. These features are common to the assessed packages and underlie more advanced calculations; for example, temperature-dependent phonons;[16,22] four-phonon scattering;[23–25] scattering by defects,[26,27] boundaries,[28–30] and electrons;[31–35] and the so-called "coherent" contribution to thermal conductivity that can be obtained from the Wigner transport equation[36–38] or the quasi-harmonic Green–Kubo approach.[39]

The starting point is a crystal structure, which is relaxed to minimize the potential energy and forces for a chosen calculator (e.g., DFT or an empirical potential). Phonons are computed from harmonic lattice dynamics. The required inputs are the atomic masses and harmonic force constants, which are the second derivatives of the potential energy with respect to atomic displacements away from equilibrium. These inputs are used to build the dynamical matrix at a wave vector in the first Brillouin zone, whose diagonalization provides phonon frequencies and mode shapes. The frequencies are used to calculate the volumetric heat capacity using Bose–Einstein statistics and to build the phonon dispersion and the density of states. The group velocity vector is the gradient of the dispersion.

The calculated phonons are non-interacting. Cubic force constants are required to obtain the intrinsic three-phonon scattering rates from the Fermi golden rule. Phonon-isotope scattering is typically treated using the harmonic-level theory of Tamura.[40] The phonons and their scattering rates are then used in a solution to the PBTE [under the relaxation time approximation (RTA) or using the full scattering matrix] to solve for the phonon distribution functions and lifetimes. Thermal conductivity can then be calculated from Eq. (1). Many of the calculations presented here are at the RTA level, for which the lifetimes in Eq. (1) carry no directional dependence.

III. MATERIALS

Four materials were chosen for the benchmark calculations: germanium (Ge), rubidium bromide (RbBr), monolayer molybdenum diselenide ($MoSe_2$), and aluminum nitride (AlN), with some characteristics listed in Table I. Further information is provided in

TABLE I. Materials studied in the benchmark.

Material	Structure (space group)	Atoms in a primitive cell	Bonding type(s)	Measured k [W/(m-K)] @ 300 K, naturally occurring (isotopically pure)
Ge	Diamond (Fd-3m, 227)	2	Covalent	62 (73 for ^{70}Ge)[41]
RbBr	Rock salt (Fm-3m, 225)	2	Covalent, ionic	3.2–3.4[42,43]
$MoSe_2$	2D hexagonal (P-6m2, layer group 78)	3	Covalent, ionic	~60[44]
AlN	Wurtzite ($P6_3mc$, 186)	4	Covalent, ionic	316 (c axis)[45]

Sec. S1 of the supplementary material. These materials, which have relatively straightforward structures and electronic behaviors, cover a range of structure types, symmetries, bonding environments, and compositions, with measured thermal conductivities that span from 3 to 300 W/(m-K) around room temperature.

Germanium is a simple material with a diamond structure that has a modest room temperature thermal conductivity. High-quality, naturally occurring (with five isotopes) and isotopically purified samples (^{70}Ge) have been characterized, such that reliable dispersion and temperature-dependent thermal conductivity data are available.

Rubidium bromide is a cubic alkali halide rock salt compound that also has reliable measured dispersion and thermal conductivity data available. It has an order of magnitude lower thermal conductivity than Ge, likely due to softer ionic bonding. Both Rb and Br have two naturally occurring isotopes. Long-range dipole corrections that underlie optic branch splittings will be important for the phonon calculations.[46,47]

Monolayer molybdenum diselenide is an example of a two-dimensional (2D) hexagonal material in a larger family of transition metal dichalcogenides. Molybdenum has seven naturally occurring isotopes, while selenium has six. As with the majority of 2D monolayers, reliable measurements are not available for the thermal conductivity of $MoSe_2$, as questions remain regarding sample quality and size, strain, substrate effects, and measurement uncertainty. $MoSe_2$ was chosen, in part, because of a lack of reference data, experimental or theoretical, and thus less distraction to the teams. Calculating the thermal conductivity of a 2D material offers additional challenges than those present for the other materials in the benchmark, which are all three-dimensional. These challenges include realizing the quadratic shape of the acoustic flexure branch, which impacts the structural stability and the low-frequency phonon–phonon scattering, and obtaining convergence with the vacuum space size.[48–50]

Aluminum nitride is well-characterized experimentally. It is anisotropic (hexagonal wurtzite crystal structure), and its strong bonds (partially covalent, partially ionic) lead to the highest thermal conductivity values of the studied materials. As with RbBr, long-range dipole corrections will be important. Phonon-isotope scattering is negligible.

IV. PROCESS

A. Open-source packages

The packages to be benchmarked are ALAMODE,[5] phono3py,[6,7] and ShengBTE.[8] These packages were chosen from a larger pool of similar packages based on the number of citations they have received. These packages all

- use permutation and space group symmetries to reduce the number of distinct force constants.
- obtain force constants, with translational invariance enforced, internal and/or external to the package. Available techniques include density functional perturbation theory (DFPT) (harmonic only), finite differences, and/or linear regression. The latter two techniques involve moving some number of atoms in a supercell or a set of supercells.
- can handle long-range interactions.
- calculate three-phonon scattering rates.
- calculate phonon-isotope scattering rates using the Tamura formulation.[40]
- ensure energy conservation in the three-phonon and phonon-isotope scattering events using Gaussian functions (fixed broadening or using an adaptive broadening technique) and/or the tetrahedron method.[51]
- solve the PBTE under the RTA. phono3py and ShengBTE also solve the PBTE using the full scattering matrix.

All the packages are fully deterministic, such that the same outputs will be obtained for the same inputs, so long as the package version is the same. Full details about each package can be found in its official documentation.

B. Teams

Two teams were selected for each of the three transport packages by the organizers (AJHM and LL). One team consisted of the package developer(s). The other team consisted of expert users of that package, who were identified based on their publication record. The teams and their members are listed in Table II.

C. Chronology

The chronology is shown in Fig. 1. A kick-off meeting that included all participants was held in December 2021. At this meeting, the "Free Phase" was introduced. The six teams were first charged with studying Ge (December 2021–February 2022). After submitting their results and receiving feedback from the organizers, they studied RbBr and monolayer $MoSe_2$ (March 2022–June 2022). The phono3py Developer team did not perform calculations for RbBr and monolayer $MoSe_2$. Teams were asked not to communicate with each other but were encouraged to interact with the organizers. The Free Phase, thus, resulted in five or six independent

TABLE II. Developer and Expert teams for each package. The team leaders are identified in bold. The DFT package used by each team is also provided [either Quantum Espresso (QE)[52,53] or VASP[54–56]].

Package	Developer team	Expert team
ALAMODE	Ryota Masuki and **Terumasa Tadano** (VASP)	Tomu Hamakawa, Han Meng, Cheng Shao, and **Junichiro Shiomi** (QE and VASP)[a]
phono3py	**Atsushi Togo** (VASP)	**Tribhuwan Pandey** (VASP)
ShengBTE	**Wu Li** and Fanchen Meng (QE)	**Hua Bao**, Shouhang Li, Ao Wang, and Xinyu Zhang (QE)

[a]For consistency with the ALAMODE Developer team, only the VASP-based results from the ALAMODE Expert team are included in the subsequent analysis and discussion. Their QE-based results are provided in Sec. S2 of the supplementary material.

predictions of phonon properties and thermal conductivity for each of the three materials, which were then analyzed by the organizers.

In August 2022, a meeting was held to present the results of the Free Phase to all participants and to receive their feedback. The next stage was the "Collaborative Phase." The two teams for each package were combined, such that there were now three teams in total. The organizers met individually with these three teams in October 2022 to solicit more feedback on the process. The teams were tasked to apply what they had learned from the Free Phase to first study Ge (October 2022–December 2022, to determine if discrepancies from the Free Phase could be resolved) and then AlN (January 2023–March 2023). As with the Free Phase, the three teams were asked not to interact with each other but had full access to the organizers. The Collaborative Phase resulted in three independent predictions of phonon properties and thermal conductivity for each of the two materials, which were then analyzed by the organizers.

At the end of the Free Phase, the DFT and force constant calculations were identified as possible sources of discrepancies between the phonon properties and thermal conductivities calculated by the different teams. As such, during the Collaborative Phase, the three Developer teams also performed calculations on Ge using the same set of force constants (October 2022–November 2022), so as to isolate the role of the PBTE solver in the three packages.

D. Approach

The teams were provided with a checklist for each material, which are provided in Sec. S1 of the supplementary material. As an example, an abridged version for the Collaborative Phase study of Ge is provided in Table III. The only hard constraints were the pseudopotential(s) and the exchange-correlation functional to be used in the DFT calculations, so that variations in calculations could not be attributed to these choices. The Perdew–Burke–Ernzerhof solids (PBEsol) projector augmented wave (PAW) formalism was used for all materials except RbBr, for which no

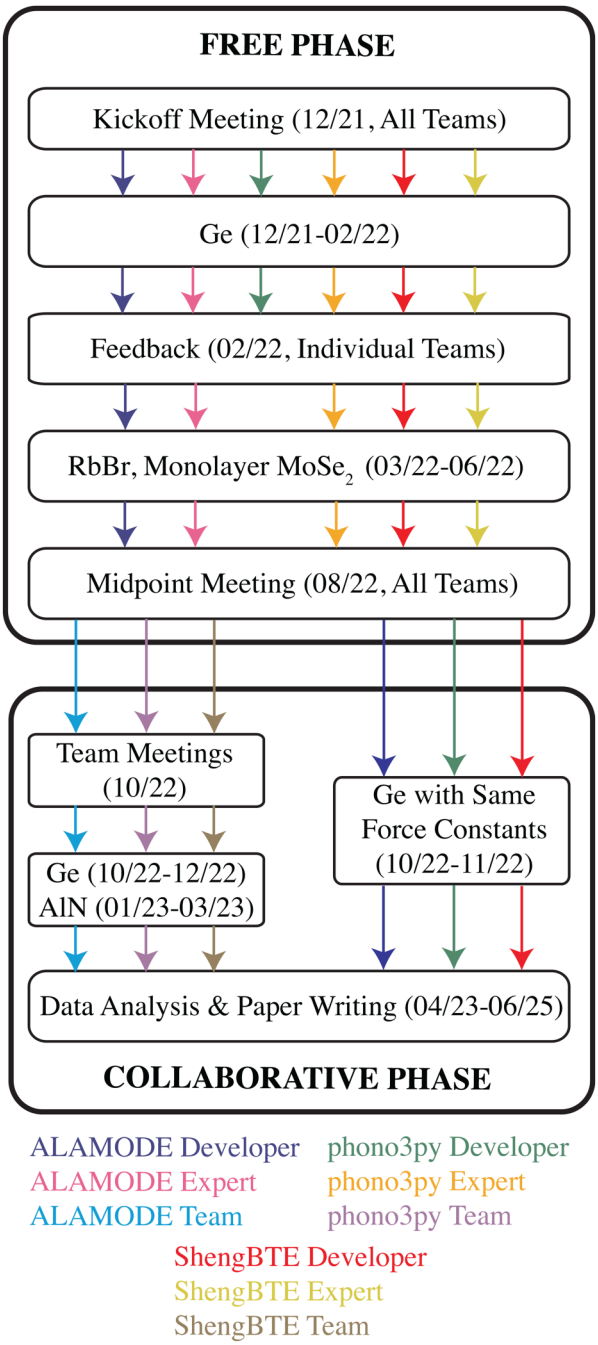

FIG. 1. Chronology of events. The color for each team is used in subsequent figures.

PBEsol pseudopotential file was available for Rb in the online Quantum Espresso (QE)[52,53] repository. For RbBr, all teams used PBE PAW. Otherwise, the teams were free to select the DFT package, with all teams using QE or VASP[54–56] (Table II). Each

TABLE III. Abridged Ge checklist for the collaborative phase.

Germanium	
Space group	Fd-3m, 227
Lattice vectors	$\mathbf{R}_1 = (-a/2, 0, a/2)$, $\mathbf{R}_2 = (0, a/2, a/2)$, $\mathbf{R}_3 = (-a/2, a/2, 0)$
Atomic positions	$Ge_1 = (0,0,0)$, $Ge_2 = (a/4, a/4, a/4)$
Isotopes	20.38% ^{70}Ge (69.924 amu), 27.31% ^{72}Ge (71.922 amu), 7.76% ^{73}Ge (72.923 amu), 36.72% ^{74}Ge (73.921 amu), 7.83% ^{76}Ge (75.921 amu), use ^{70}Ge for isotopically pure calculations
DFT	PBEsol PAW, no *d* states in valence Quantum Espresso: Ge.pbesol-n-kjpaw_psl.1.0.0.UPF VASP: standard "Ge" version with a pbesol flag in INCAR file
Structure	
Relaxed $T = 0$ K lattice constant (a)	Target accuracy <0.005 Å
Methods/convergence	Energy/force thresholds, integration mesh/grid shifting, smearing
Phonons	
Harmonic force constants	Supercell perturbations: supercell size, displacement size, symmetries applied, invariance constraints DFPT: coarse grid, symmetries applied, invariance constraints
Dispersion	Target accuracy < 0.1 THz for **Γ**, **X**, and **L** points Three segments: **Γ** → **X**, **Γ** → **K** → **X**, and **Γ** → **L**, with 100 evenly divided wave vector points per segment Normalized wave vectors (units of $2\pi/a$) and frequencies (THz) for six polarizations
Methods/convergence	Thresholds
Anharmonic transport	
Cubic force constants	Supercell size, neighbor cutoff, displacement size, symmetries applied, invariance constraints
Scattering rates	Three-phonon (RTA) and phonon-isotope at 20 and 300 K
Thermal conductivity	Evidence of convergence at 20 and 300 K for isotopically pure under RTA and full PBTE solutions. Target accuracy <2% difference between successive grids Naturally occurring and isotopically pure under RTA and full PBTE solutions. 20–50 K in increments of 10 K, 50–300 K in increments of 25 K, and 300–1000 K in increments of 100 K Accumulated with respect to frequency and mean free path at 20 and 300 K
Methods/convergence criteria	Delta function representation, integration grid

team was given access to an online repository for (i) completing a summary spreadsheet with key information and results and (ii) uploading the input files required to run all their calculations and all the requested data. All the requested information is openly available.[57]

V. RESULTS: GERMANIUM

A. Overview

This section will focus on Ge, where we have the most data sets. Selected calculation details and results are presented in Tables IV and V. The other materials are discussed in Sec. VI. The presentation will start with the dispersion and temperature dependence of thermal conductivity, then probe accumulation functions, lifetimes, and force constants. From these results, explanations will be suggested for differences between calculations, which will help to form the recommendations for best practices in Sec. VIII.

B. Transport package

We start with the Ge Developer calculations performed with the same set of harmonic and cubic force constants in each transport package. These calculations allow us to investigate the impact of the scattering rate calculations (three-phonon and phonon-isotope) and PBTE solution on thermal conductivity, isolated from details of the DFT and force constant calculations.

The phonon frequencies calculated from the three packages are identical, with the values at high symmetry points in the Brillouin zone reported in Table V. The isotopically pure ^{70}Ge RTA thermal conductivities calculated from the three transport packages are plotted vs temperature in Fig. 2(a) (solid curves). All teams found that a $32 \times 32 \times 32$, hereafter abbreviated as 32×, phonon wave vector (**q**)-grid was sufficient to remove size effects. Between temperatures of 50 and 1000 K, the spread in the three calculations around their mean value is less than ±1%. The corresponding 300 K thermal conductivity accumulations as a function of frequency, f, are plotted in Fig. 2(b). The three solid curves have the same fine structure, and the total thermal conductivities at this temperature fall within a range of 0.7 W/(m-K) [51.6–52.3 W/(m-K)]. These results indicate a strong consistency in the three-phonon scattering rate calculations implemented in the transport packages.

Between temperatures of 200 K and 1000 K, the isotopically pure RTA thermal conductivities follow a $T^{-1.05}$ scaling, which is

TABLE IV. Comparison of Ge calculation decisions.

	Energy cutoff (eV)[b]	Force constants (harmonic/cubic)[a]			Displacement (Å)	Converged **q**-grid for *k*
		Atoms in supercell	**k**-grid	Cutoff[c]		
ALAMODE						
Free—Developer (VASP 6.2.1, ALAMODE 1.3.0)	300	216/64	2×/4×	All atoms/3nn	0.01/0.03	50 × (300 K)
Free—Expert (VASP 5.4.4, ALAMODE 1.1.0)	225	64/64	10×/5×	All atoms/3nn	0.04/0.06	50 × (300 K)
Collaborative (VASP 6.4.0, ALAMODE 1.4.1)	225	216/216	7×/4×	All atoms/3nn	0.01/0.02	50 × (20 K) 50 × (300 K)
phono3py						
Free—Developer (VASP 6.2.1, phonopy 2.14.0[d], phono3py 2.3.0[d])	240	512/64	2×/4×	All atoms/all atoms	0.03/0.03	43 × (300 K)
Free—Expert (VASP 6.2.1, phonopy 2.12.0, phono3py 2.1.0)	600 (H), 550 (C)	432/128	2×/3×	All atoms/all atoms	0.01/0.03	41 × (300 K)
Collaborative (VASP 6.2.1, phonopy 2.12.0, phono3py 2.1.0)	600 (H), 550 (C)	432/128	2×/3×	All atoms/all atoms	0.01/0.03	51 × (20 K) 41 × (300 K)
ShengBTE						
Free—Developer (QE 6.6, ShengBTE 1.2.0)	898	DFPT/250	16×/1×	…/4nn	…/0.01	32×(300 K)
Free—Expert (QE 6.7, ShengBTE 1.1.1)	1088	DFPT/128	16×/2×	…/5nn	…/0.01	32×(300 K)
Collaborative (QE 6.6, ShengBTE 1.2.0)	898	DFPT/250	16×/1×	…/10nn	…/0.01	34 × (20 K) 30 × (300 K)
Developer same force constants						
VASP 6.3.1, phonopy 2.14.0, phono3py 2.3.2	240	250/128	2×/2×	All atoms/all atoms	0.01/0.03	32 × (All Teams)

[a]In cells where there are two entries separated by a forward slash (/), the first entry corresponds to the harmonic force constants and the second entry corresponds to the cubic force constants.
[b]Unless noted, the same value was used for the harmonic (H) and cubic (C) force constant calculations.
[c]nn, nearest neighbor.
[d]Development versions, which should be closest to phonopy 2.14.0 and phono3py 2.3.0.

close to the T^{-1} scaling expected in the presence of only three-phonon scattering and classical (i.e., Maxwell-Boltzmann) statistics. Between temperatures of 50 and 100 K, the thermal conductivities scale as $T^{-2.2}$, pointing to the impact of quantum statistics well below Ge's Debye temperature of 374 K. While temperature scalings stronger than T^{-1} have been reported in materials that display hydrodynamic phonon transport in the Ziman regime,[60–62] these effects only become apparent in a full PBTE solution, where normal processes are not treated as being purely resistive.

In the initial set of these Ge Developer calculations, all neighbors in the 128-atom supercell were included when calculating the harmonic and cubic force constants. This choice leads to ambiguity when defining some interactions outside the supercell and thus breaking of derivative permutation symmetry.[63,94] In Fig. 2(b), a second ALAMODE calculation is presented, where the cubic force constants were truncated at the third nearest neighbor (nn) (i.e., all considered interactions are contained within the supercell). The resulting thermal conductivity is higher than the first ALAMODE calculation (4.4 W/(m-K) higher at a temperature of 300 K), suggesting the sensitivity of the thermal conductivity to the cubic force constants and their symmetries.

The ShengBTE and phono3py isotopically pure thermal conductivities calculated using the full scattering matrix in the PBTE solution are plotted vs temperature in Fig. 2(a) (dashed curves). ALAMODE does not provide a full scattering matrix PBTE solution. At a temperature of 50 K, the spread of the two calculations around their mean value is less than ±4%, and for temperatures between 100 and 1000 K, the spread is ±3% or less. The PBTE is solved in ShengBTE using an iterative approach, while phono3py implements a direct solution, which is a possible reason for the larger spread compared to the RTA thermal conductivities.

The 300 K lifetimes for isotopically pure Ge (i.e., only limited by three-phonon interactions) are plotted in Fig. 3. These lifetimes were calculated on the same 32 × **q**-grid so that they can be directly compared. While variations in the fine structure are apparent, all calculations give the same general trends with frequency. The spread at a given frequency is related to polarization and wave vector dependencies.

TABLE V. Selected Ge results.

		Phonon frequency (THz)			k @ 300 K [W/(m-K)]	
	a (Å)	f_Γ	f_X	f_L	k_{pure}	$k_{natural}$
ALAMODE						
Free—Developer	5.702	8.49	2.10, 6.90, 7.87	1.70, 6.36, 6.97, 8.30	61.6 (RTA)	53.1 (RTA)
Free—Expert	5.702	8.65	2.07, 6.89, 7.86	1.66, 6.35, 6.96, 8.29	54.2 (RTA)	46.6 (RTA)
Collaborative	5.702	8.66	2.10, 6.90, 7.87	1.73, 6.21, 6.95, 8.33	60.4 (RTA)	52.0 (RTA)
phono3py						
Free—Developer	5.702	8.71	2.11, 6.86, 7.87	1.71, 6.37, 6.94, 8.29	52.0 (RTA), 55.1 (full)	45.5 (RTA), 47.2 (full)
Free—Expert	5.703	8.56	2.11, 6.90, 7.87	1.70, 6.34, 6.96, 8.29	51.9 (RTA), 55.5 (full)	45.6 (RTA), 47.7 (full)
Collaborative	5.703	8.56	2.11, 6.90, 7.87	1.70, 6.34, 6.96, 8.29	53.3 (RTA), 56.9 (full)	46.8 (RTA), 49.0 (full)
ShengBTE						
Free—Developer	5.687	8.62	2.11, 6.93, 7.85	1.71, 6.39, 6.93, 8.31	57.9 (RTA), 61.8 (full)	49.7 (RTA), 51.8 (full)
Free—Expert	5.686	8.63	2.08, 6.95, 7.85	1.70, 6.39, 6.94, 8.32	59.4 (RTA), 62.7 (full)	52.5 (RTA), 54.3 (full)
Collaborative[a]	5.687	8.63	2.12, 6.94, 7.86	1.72, 6.40, 6.94, 8.32	60.4 (RTA), 64.0 (full)	52.2 (RTA), 54.2 (full)
Same force constants	5.702					
ALAMODE 1.4.2		8.72	2.24, 6.91, 7.93	1.75, 6.40, 7.01, 8.33	51.6 (RTA)	44.4 (RTA)
phono3py 2.9.2		8.72	2.24, 6.91, 7.93	1.75, 6.40, 7.01, 8.33	52.1 (RTA), 55.4 (full)	44.9 (RTA), 46.8 (full)
ShengBTE 1.2.0		8.72	2.24, 6.91, 7.93	1.75, 6.40, 7.01, 8.33	52.3 (RTA), 54.6 (full)	45.1 (RTA), 47.1 (full)
Experiment[41,58,59]	5.653–5.658 (8–300 K)	9.12	2.40, 7.21, 8.26	1.90, 6.66, 7.34, 8.70	73 (^{70}Ge)	62

[a]The ShengBTE Collaborative Phase thermal conductivities are taken from their 34× **q**-grid.

The phonon-isotope scattering rates and naturally occurring RTA thermal conductivities were also calculated using the three packages. The structure of the phonon-isotope scattering rate output files is the same in ALAMODE and phono3py, allowing for a direct comparison. 99% of more than 5000 phonon modes have phonon-isotope scattering rates that fall within ±5% of their average value. Differences are likely a result of a small difference in how the Tamura theory is implemented.[64] Between temperatures of 100 and 1000 K, the spread of the three naturally occurring thermal conductivity calculations around their mean value is less than ±1%. This small spread, which is similar to that for the isotopically pure RTA thermal conductivities, suggests that the small differences in the mode-wise phonon-isotope scattering rates even out across the full spectrum.

In the remainder of the paper, we focus on the RTA solution of the PBTE to allow for a comparison of the three transport packages. Furthermore, we show a mixture of calculations for isotopically pure and naturally occurring compositions of all materials, focusing the discussion on the anharmonic scattering.

C. Free and collaborative phases

1. Process

After receiving the Ge results in the Free Phase from the six teams, the organizers assessed the submissions. In some cases, the teams were asked to make immediate modifications, for example, re-plotting the dispersion curves along the same defined paths in the Brillouin zone and using consistent masses. In other cases, changes were suggested for the subsequent materials, for example, ensuring that the Developers and Experts use the same version of the transport package.

2. DFT calculations

The teams relaxed the Ge structure using the structural and DFT input parameters defined in Table III. The VASP calculations gave a lattice constant, a, of 5.702–5.703 Å, while the QE calculations gave 5.687 Å. These zero-temperature values can be compared with the measured values of 5.653–5.658 Å in going from 8 to 300 K.[59] The larger calculated lattice constant is typical of PBE

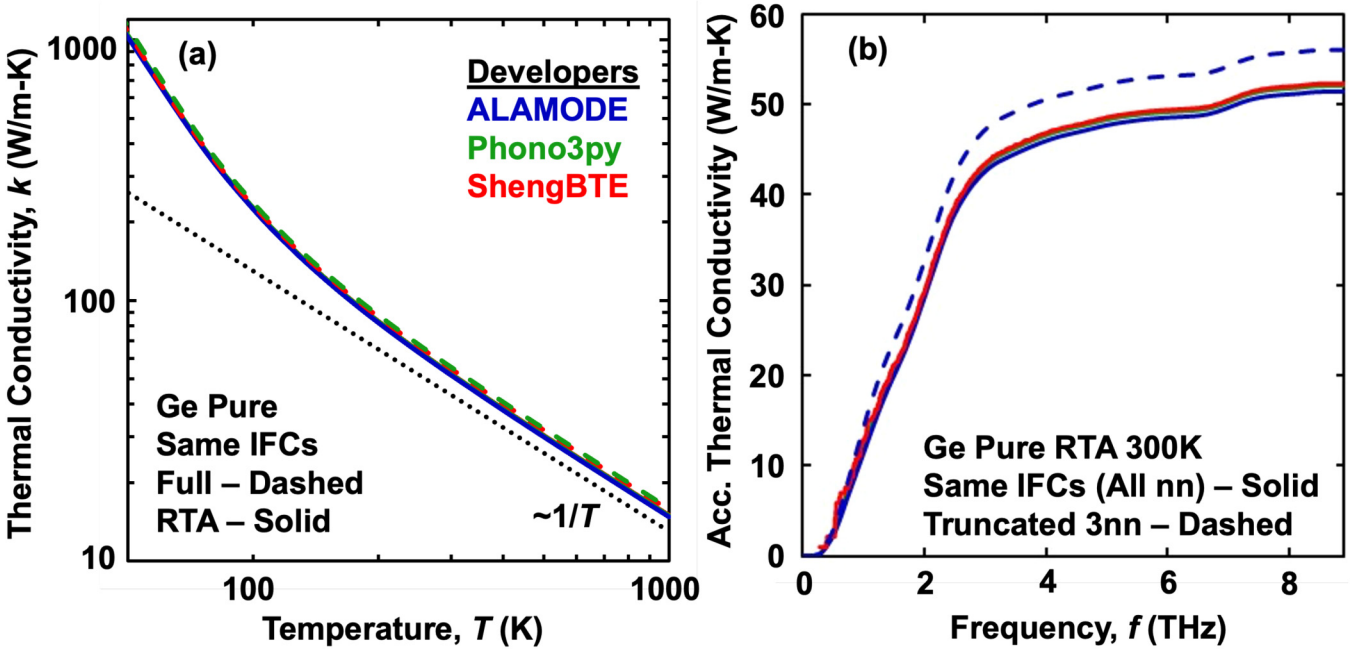

FIG. 2. Ge Developer calculations performed using the same set of harmonic and cubic force constants. (a) Temperature dependence of RTA and full PBTE solution thermal conductivities for isotopically pure ^{70}Ge. (b) RTA thermal conductivity accumulation with frequency at a temperature of 300 K for isotopically pure ^{70}Ge.

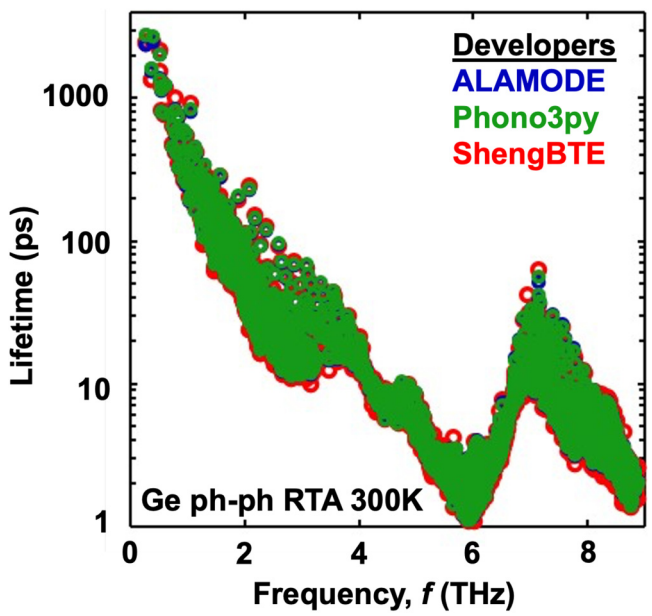

FIG. 3. Ge Developer calculations of 300 K three-phonon scattering lifetimes performed using the same set of harmonic and cubic force constants and a 32 × **q**-grid.

generalized gradient approximation (GGA) exchange-correlation functionals in DFT and results in phonons with lower frequencies than obtained in measurements (described below and see Table V).[65] A further discussion on comparing the calculations for Ge and the other materials to experimental measurements is provided in Sec. VII. Despite variations in the DFT input parameters [e.g., smearing and electronic wave vector (**k**)-grid] and convergence criteria [e.g., plane wave energy cutoff and energy convergence threshold], the structural results are remarkably similar. Furthermore, little variation is seen when comparing the electronic band structures of all the calculations.

3. Phonon dispersion

The dispersion curves along selected high-symmetry directions are plotted in Figs. 4(a)–4(c). Each sub-figure contains the results from the Free and Collaborative Phases for a given transport package. All calculations employed acoustic sum rules to enforce translational invariance for the harmonic force constants. While the acoustic phonon frequencies for the three calculations for a given transport package are generally close, differences are present in the optic phonon frequencies for ALAMODE and phono3py.

The ShengBTE phonons were all determined using DFPT in QE, with the same **k**-grid (16×) and similar input **q**-grids (either 6× or 7×). There is no visual difference in the dispersion curves plotted in Fig. 4(c). From Table V, the phonon frequencies at a specified wave vector and polarization all fall within 0.04 THz.

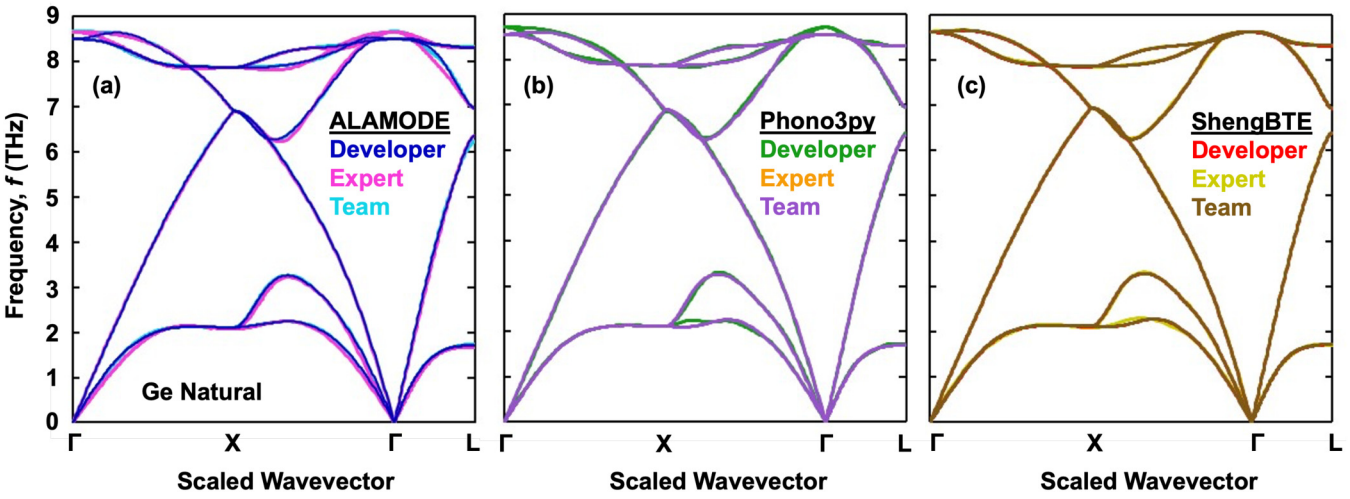

FIG. 4. Ge dispersion from the Free (Developer and Expert) and Collaborative (Team) Phases from (a) ALAMODE, (b) phono3py, and (c) ShengBTE.

The ALAMODE harmonic force constants were obtained using VASP by displacing one atom in a supercell and using linear regression. In the Free Phase, the Developer used a 216-atom supercell with a 0.01 Å displacement and a 2× k-grid, while the Expert used a 64-atom supercell with a 0.04 Å displacement and a 10× k-grid. In the Collaborative Phase, the team used a 216-atom supercell with a 0.01 Å displacement with a 7× k-grid. Differences in the frequencies are apparent; for example, the spread is 0.17 THz for the optic mode at the **Γ**-point and 0.14 THz for the longitudinal acoustic mode at the **L**-point.

The phono3py harmonic force constants were also obtained using VASP by the linear regression method,[66] with all calculations using a 2× k-grid. In the Free Phase, the Developer used a 512-atom supercell with 0.03 Å displacements, while the Expert used a 432-atom supercell with 0.01 Å displacements. The Collaborative Phase calculations were the same as those from the Expert in the Free Phase. Differences in some frequencies are apparent, while others are very close; for example, the spread is 0.16 THz for the optic mode at the **Γ**-point.

Encouragingly, the three sets of dispersion curves from the Collaborative Phase line up well, with frequency spreads for the modes listed in Table V ranging from 0.01 to 0.18 THz.

4. Thermal conductivity

The temperature dependence of the RTA thermal conductivity for isotopically pure Ge is plotted in Fig. 5(a) for the Free Phase and in Fig. 5(b) for the Collaborative Phase. Data between temperatures of 100 and 1000 K are plotted and considered in the ensuing analysis. The **q**-grid choice, which was based on convergence studies at 300 K in the Free Phase and at 20 and 300 K in the Collaborative Phase, may lead to size effects at low temperatures. Considering all Free Phase and Collaborative Phase data together, there is no discernible trend in the thermal conductivities with the converged **q**-grid sizes.

For a given transport package, the spread in the two Free Phase thermal conductivities around their mean at a given temperature is less than ±2% for ShengBTE, less than ±1% for phono3py, and less than ±6% for ALAMODE. For each transport package, one of the Developer or Expert thermal conductivities is systematically higher than the other.

Considering all the Free Phase data together, the six thermal conductivity sets fall within a range around their mean that starts at ±13% at a temperature of 100 K (223–281 W/m K) and decreases to ±8%–9% between temperatures of 300 and 1000 K (e.g., at 300 K, 51.9–61.6 W/m K). The phono3py thermal conductivities are the lowest, possibly due to not using a cutoff for the anharmonic interactions.[63] There is no discernible trend between the ALAMODE and ShengBTE results.

In moving from the Free Phase to the Collaborative Phase, the teams made changes in their calculations, as shown in Table IV. Team ALAMODE used a larger supercell and smaller displacements for obtaining the cubic force constants. Team phono3py used a finer **q**-grid for the thermal conductivity calculation. Team ShengBTE used more neighbors when calculating the cubic force constants. In the Collaborative Phase, the ALAMODE and ShengBTE isotopically pure RTA thermal conductivities fall within 0.2 W/m K between temperatures of 200 and 1000 K. Below 200 K, the difference increases as temperature decreases, which may be due to the different **q**-grids used by these two teams (Table IV). The phono3py thermal conductivity calculations (no anharmonic cutoff) are systematically about 12% lower than the ALAMODE and ShengBTE results over the temperature range of 200–1000 K. At a temperature of 300 K, the thermal conductivities are 60.4 W/m K (ALAMODE), 53.3 W/m K (phono3py), and 60.4 W/m K (ShengBTE).

The 300 K thermal conductivity accumulations as function of frequency for naturally occurring Ge are plotted in Fig. 6(a) for the Free Phase and in Fig. 6(b) for the Collaborative Phase. The spread in the total thermal conductivities is discussed in the previous

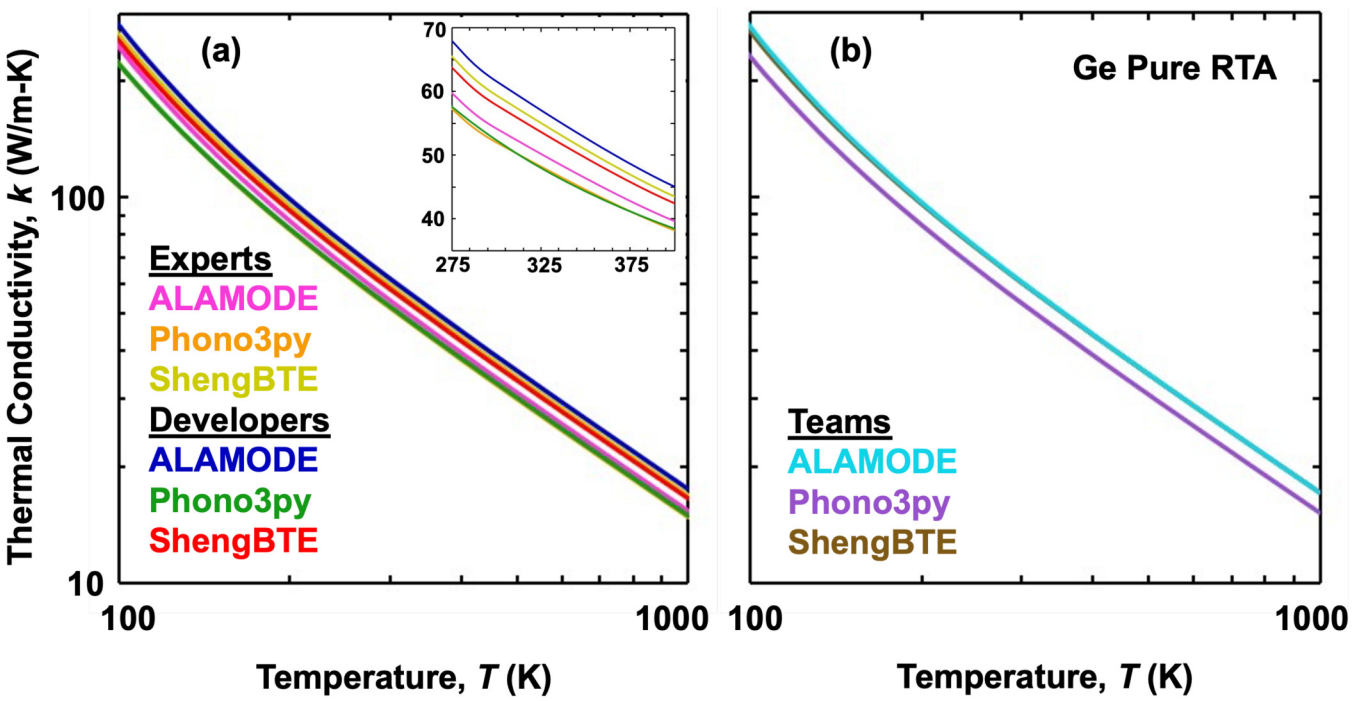

FIG. 5. Isotopically pure Ge RTA thermal conductivity in (a) the Free Phase and (b) the Collaborative Phase.

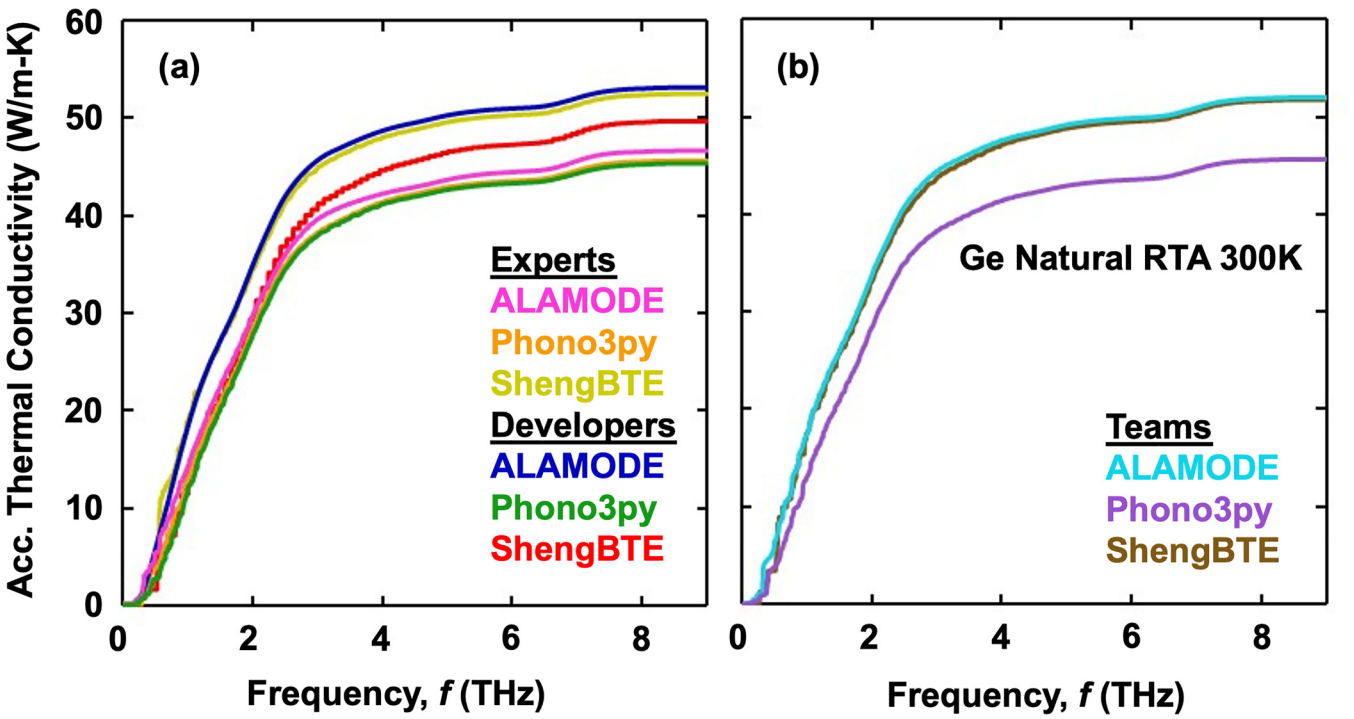

FIG. 6. Naturally occurring Ge RTA thermal conductivity accumulation as a function of frequency at 300 K in (a) the Free Phase and (b) the Collaborative Phase.

paragraphs. All nine accumulation functions show a rapid increase with frequency up to about 3 THz followed by a more gradual increase up to the maximum frequency. Differences are prominent in the low-frequency regime, while the behavior is similar in the high-frequency regime. In the Free Phase data, the 9% spread around the mean for frequencies greater than 3 THz is similar to that for the total thermal conductivity. With decreasing frequency, this spread increases dramatically: 15% at 2 THz, 30% at 1 THz, and >100% below 0.5 THz. The increasing spread is primarily a result of the sampling of low-frequency acoustic phonons. The calculations giving the highest overall thermal conductivities also have the steepest low-frequency thermal conductivity accumulations, demonstrating the importance of the low-frequency acoustic phonons.

5. Three-phonon scattering lifetimes and cubic force constants

From Eq. (1), differences in calculated thermal conductivities must originate from the modal heat capacities, group velocities, and/or lifetimes. Because the differences in the phonon frequencies from all the calculations are small (Table V), heat capacity and group velocity effects are unlikely to drive the observed range of thermal conductivities. The lifetimes, and thus the scattering rates, are the most likely culprit.

Based on the frequency-dependent thermal conductivity accumulation functions shown in Figs. 6(a) and 6(b), we now examine the three-phonon scattering lifetimes in the low-frequency (<1 THz) regime. The low-frequency thermal conductivity accumulations for naturally occurring Ge at a temperature of 300 K for the Collaborative Phase are plotted in Fig. 7(a). Most of the differences in the accumulations, and thus the overall thermal conductivity, occur in this frequency region. The ShengBTE integration grid is the sparsest (30×, compared to 50× for ALAMODE and 41× for phono3py) so that the smaller number of low-frequency modes carry more weight in their contributions. The corresponding three-phonon-scattering lifetimes are plotted in Fig. 7(b) as a function of frequency. At 0.75 THz and higher, the lifetimes generally agree and differences in the thermal conductivity accumulations are relatively constant. Below 0.75 THz, the phono3py lifetimes are generally lower than the ALAMODE lifetimes, which is reflected in the generally lower thermal conductivity accumulation for phono3py. Large mode lifetimes [encircled in Fig. 7(b)] can be correlated with rapid increases in the accumulations for the ALAMODE and ShengBTE curves at 0.3 and 0.55 THz, respectively. The variations in the lifetimes and low-frequency thermal conductivity accumulations can be partially attributed to the use of different **q**-grids, where polarization and wave vector dependencies can become apparent. The variations in the thermal conductivity accumulations average out with increasing frequency, as more modes are included in the summations per unit frequency.

It may be tempting to blame low-frequency variations in the three-phonon scattering on variations in the enforcement of translational invariance on the cubic force constants.[67] Each package, however, applies these conditions to numerical precision. We did not verify whether other symmetry constraints were determined to the same accuracy. The eight largest irreducible cubic force constants for the Collaborative Phase calculations are presented in Table VI. Also

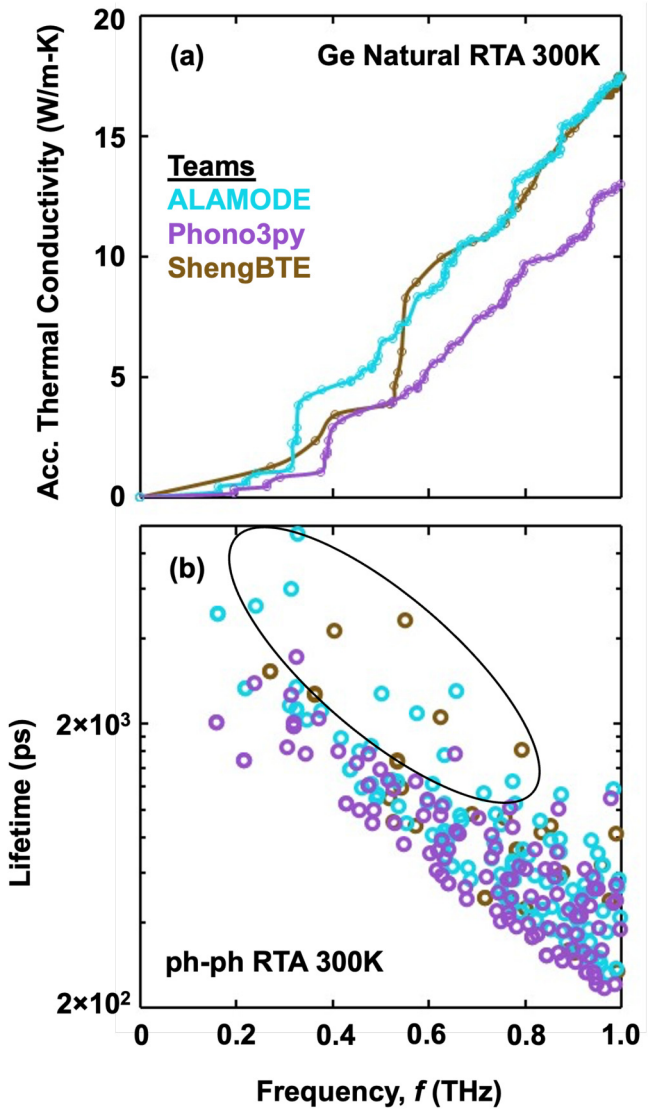

FIG. 7. Naturally occurring Ge RTA 300 K (a) thermal conductivity accumulation as a function of frequency and (b) three-phonon scattering lifetimes, up to a frequency of 1 THz.

included are the values for the Developer calculations performed using the same force constants (Sec. V B). The values are remarkably similar, though the phono3py terms are generally larger, which could be related to its smaller lifetimes seen in Fig. 7(b).

Consistent with our finding, Xie *et al.* found that the thermal conductivities of silicon, graphene, and silicene calculated from empirical potentials are sensitive to the cubic force constants.[68] In their silicon calculation, when the force accuracy was 10^{-6} eV/Å, the calculated thermal conductivity can yield a 20% error. After imposing translational invariance conditions, the error can be reduced to less than 2%. When the force accuracy was 10^{-5} eV/Å,

TABLE VI. Eight largest cubic force constants in Ge (eV/Å^3). The "Same FCs" are those from Sec. V B. The other three columns are from the Collaborative Phase. More details are provided in Sec. S3 of the supplementary material, describing the unit cells, atoms, and displacement directions for these force constants.

	Same FCs	ALAMODE	phono3py	ShengBTE
1	26.776	26.770	26.782	26.698
2	6.746	6.760	6.785	6.784
3	4.843	4.849	4.851	4.784
4	4.693	4.717	4.730	4.659
5	2.316	2.321	2.329	2.433
6	0.204	0.216	0.209	0.191
7	0.192	0.191	0.194	0.184
8	0.188	0.185	0.187	0.174

even after imposing the translational invariance conditions, the error of thermal conductivity can still be as large as 10%.

VI. RESULTS: RbBr, MONOLAYER $MoSe_2$, AND AlN

A. Overview

We now present results for RbBr (Free Phase), monolayer $MoSe_2$ (Free Phase), and AlN (Collaborative Phase), following a similar narrative as that used for Ge in Sec. V. The feedback provided to the teams after the Ge Free Phase led to more consistency in how the calculations were carried out. As such, we focus here on a comparison between all calculations performed for a given material.

All teams handled the long-range Coulombic interactions present in these three materials using DFPT. Similar to what was found for Ge, differences in the calculated phonon frequencies, which are used to calculate the heat capacity and the group velocity, are small. The lifetimes, and thus the scattering rates, are again the key differentiators in the calculated thermal conductivities.

B. RbBr

The RbBr calculation details are provided in Table VII, and the key results are provided in Table VIII. The RbBr lattice constants fall within a range of 7.007–7.022 Å, with the VASP-based calculations at the higher end. The diagonal entries of the dielectric constant tensor are in the range of 2.456–2.467, and the Born effective charges are in the range of 1.164–1.165e (positive for Rb and negative for Br). The RbBr dispersion curves are plotted in Fig. 8(a). The maximum spread of the **Γ**, **X**, and **L** point frequencies listed in Table VIII is 0.07 THz.

The naturally occurring RbBr RTA thermal conductivities are plotted vs temperature in Fig. 8(b). The five thermal conductivity sets fall within a range around their mean of $\pm 13\%$ between temperatures of 100 and 1000 K (e.g., at 300 K, 2.67–3.46 W/m K). Each of the data sets is well modeled with a T^{-n} scaling, where $0.978 < n < 0.984$. There is no discernible trend in the thermal conductivities with the converged **q**-grid sizes. The 300 K accumulation functions as a function of frequency are plotted in Fig. 8(c). Similar to the discussion regarding Ge in Sec. V C 4, the spread of the accumulation functions reflects that of the total thermal conductivities above 1.5 THz. Below 1.5 THz, the relative spread dramatically increases to 30% at 0.5 THz and >100% below this frequency, despite the observable differences in Fig. 8(c) being most apparent above 1.5 THz.

The 300 K three-phonon scattering lifetimes corresponding to the smallest (ShengBTE-Expert) and largest (ShengBTE-Developer) thermal conductivities are plotted in Fig. 8(d) as a function of frequency. Differences are apparent across the frequency spectrum. In comparing these two calculations, the major differences are (i) The Developer used smaller thresholds, energy cutoff, and **k**-grid in

TABLE VII. Comparison of RbBr calculation decisions.

		Force constants (harmonic/cubic)[a]				
	Energy cutoff (eV)[b]	Atoms in supercell	**k**-grid	Cutoff[c]	Displacement (Å)	Converged **q**-grid for k @ 300 K
ALAMODE						
Developer (VASP 6.2.0, ALAMODE 1.3.0)	300	64/64	2×/2×	All atoms/14nn	0.01/0.03	30×
Expert (VASP 6.3.0, ALAMODE 1.0.0)	290	64/64	2×/2×	All atoms/3nn	0.04/0.08	30×
phono3py						
Expert (VASP 6.2.1, phonopy 2.12.0, phono3py 2.1.0)	600 (H), 550 (C)	250/128	2×/3×	All atoms/all atoms	0.01/0.03	41×
ShengBTE						
Developer (QE 6.6, ShengBTE 1.2.0)	898	DFPT/250	6×/1×	…/6nn	…/0.01	24×
Expert (QE 6.7, ShengBTE 1.2.0)	1088	DFPT/128	16×/2×	…/5nn	…/0.01	20×

[a]In cells where there are two entries separated by a forward slash (/), the first entry corresponds to the harmonic force constants and the second entry corresponds to the cubic force constants.
[b]Unless noted, the same value was used for the harmonic (H) and cubic (C) force constant calculations.
[c]nn, nearest neighbor.

TABLE VIII. Selected RbBr results.

		Phonon frequency (THz)[a]			k @ 300 K [W/(m-K)]	
	a (Å)	f_Γ	f_X	f_L	k_{pure}	$k_{natural}$
ALAMODE						
Developer	7.022	2.29, 3.47	0.99, 1.78, 2.35, 2.45	1.67, 1.82, 2.50, 2.61	3.10 (RTA)	3.05 (RTA)
Expert	7.017	2.33 3.51	1.02, 1.80, 2.40, 2.49	1.69, 1.87, 2.55, 2.63	3.49 (RTA)	3.43 (RTA)
phono3py						
Expert	7.022	2.28, 3.47	0.99, 1.79, 2.35, 2.44	1.67, 1.80, 2.49, 2.61	2.94 (RTA), 4.15 (full)	2.89 (RTA), 4.04 (full)
ShengBTE						
Developer	7.015	2.29, 3.48	1.04, 1.83, 2.38, 2.48	1.72, 1.81, 2.50, 2.67	3.54 (RTA), 4.97 (full)	3.46 (RTA), 4.80 (full)
Expert	7.007	2.28, 3.47	0.97, 1.77, 2.36, 2.46	1.68, 1.81, 2.50, 2.62	2.71 (RTA), 4.02 (full)	2.67 (RTA), 3.92 (full)
Experiment[42,43,69,70]	6.893–6.924 (300–413 K)	2.82, 3.88	1.00, 1.78, 2.86, 2.96	2.08 (TA), …, 2.77 (LA), …		3.2–3.4

[a]The experimental phonon frequencies are at a temperature of 80 K.

their phonon calculations. Given the similarities in the phonon dispersions, these decisions are unlikely to have a major effect on the thermal conductivities. (ii) The Developer used a larger supercell (250 atoms vs 128 atoms) and a larger cutoff (6nn vs 5nn) for the cubic force constant calculations.

C. Monolayer $MoSe_2$

The monolayer $MoSe_2$ calculation details are provided in Table IX, and the key results are provided in Tables X and XI. The lattice constants (3.267–3.270 Å) and Se layer separations (2Δ) (3.328–3.332 Å) both fall within tight ranges.

The dielectric constants (in-plane and cross-plane) and z-direction Born effective charges show a range of values. The key difference in these calculations was the choice of the cross-plane system size (which sets the amount of vacuum space), which ranged from 14.3 Å to 40.0 Å. The dielectric tensor components decrease with increasing vacuum space (7.90–3.46 for in-plane and 1.64–1.16 for cross-plane). The effect of the cross-plane system size on the dielectric constants can be corrected.[71] Upon doing so, the dielectric constant ranges reduce to 15.74–15.81 (in-plane) and 6.11–6.19 (cross-plane). The magnitudes of the z Born effective charges for Mo and Se decrease with increasing vacuum space.

The $MoSe_2$ dispersion curves are plotted in Fig. 9(a). The spread of the five calculations for the five **Γ**-point frequencies ranges from 0.04 to 0.14 THz (Table X). We fit the first 10% of the $\mathbf{\Gamma} - \mathbf{M}$ acoustic flexure branch from each team with a second-order polynomial. The ratio of the linear coefficient to the quadratic coefficient ranged from 0.001–0.04 (arbitrary units) for the five dispersions. This result confirms the expected quadratic behavior.

The naturally occurring $MoSe_2$ RTA thermal conductivities are plotted vs temperature in Fig. 9(b). The five thermal conductivity sets fall within a range around their mean of ±7% between temperatures of 100 and 1000 K [e.g., at 300 K, 65.5–73.8 W/(m-K)]. Each of the data sets is well modeled with a T^{-n} scaling, where $1.078 < n < 1.085$. There is no discernible trend in the thermal conductivities with the converged **q**-grid sizes. Thermal conductivity shows a weak positive correlation with increasing cross-plane system size. The 300 K thermal conductivity accumulation functions as a function of frequency are plotted in Fig. 9(c). The ALAMODE Developer curve is lower than the other curves starting from the lowest frequencies. The other four curves begin to show separation around a frequency of 2 THz.

The 300 K three-phonon scattering lifetimes are plotted in Fig. 9(d) as a function of frequency for the ALAMODE Developer (lowest thermal conductivity) and ALAMODE Expert (second-highest thermal conductivity) calculations. Clear differences can be seen for frequencies below 0.5 THz, which lead to the differences seen in the low-frequency thermal conductivity accumulations. As seen in Table IX, there are numerous differences in the Developer and Expert cubic force constant calculations, including the supercell size, the **k**-grid, the cutoff, and the displacement size. The Expert also used a larger cross-plane system size than the Developer (40.0 Å vs 18.3 Å).

D. AlN

The AlN calculation details are provided in Table XII, and the key results are provided in Table XIII. The lattice constants a (3.113–3.116 Å) and c (4.982–4.987 Å), and the internal coordinate u (0.381–0.382 Å) all fall within tight ranges. The diagonal entries of the dielectric constant tensor are in the ranges of 4.482–4.496 (x and y) and 4.712–4.727 (z). The magnitudes of the Born effective charges are in the ranges of 2.514–2.522e (x and y) and 2.678–2.685e (z) (positive for Al and negative for N). The AlN dispersion curves are plotted in Fig. 10(a). The spread of the three calculations at the two **Γ**-point frequencies where there is splitting and at the four **A**-points is at most 0.02 THz (Table XIII).

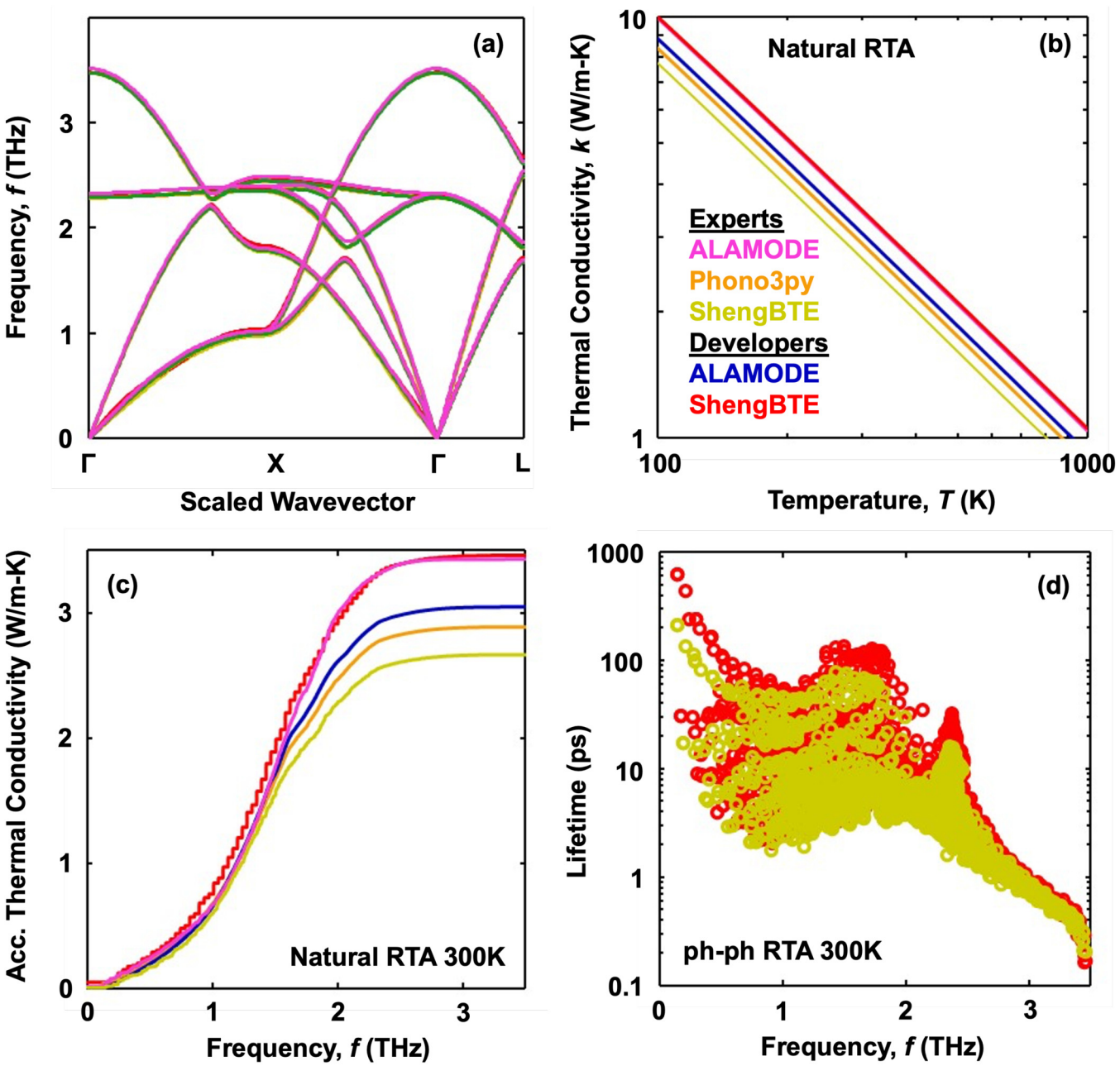

FIG. 8. RbBr results. (a) Dispersion. (b) Naturally occurring RTA thermal conductivity. (c) Frequency-dependent thermal conductivity accumulation at 300 K. (d) ShengBTE three-phonon scattering lifetimes at 300 K.

The AlN RTA thermal conductivities in the in-plane (a) and cross-plane (c) directions are plotted vs temperature in Fig. 10(b). For the in-plane direction, the three thermal conductivity sets fall within a range around their mean of $\pm 9\%$ at a temperature of 100 K that decreases to $\pm 4\%$ at a temperature of 1000 K. The range at 300 K is 263–282 W/(m-K). For the cross-plane direction, the three thermal conductivity sets fall within a range around their mean of $\pm 14\%$ at a temperature of 100 K that decreases to 5% at a temperature of 1000 K. The range at 300 K is 232–282 W/(m-K). Between temperatures of 400 and 1000 K, each of the data sets is well modeled with a T^{-n} scaling, where $1.13 < n < 1.15$. Due to AlN's high Debye temperature of 1150 K, the scaling is stronger at lower temperatures, as was found for Ge.

TABLE IX. Comparison of monolayer $MoSe_2$ calculation decisions.

	Energy cutoff (eV)[b]	Cross-plane system size (Å)	Force constants (harmonic/cubic)[a]			Displacement (Å)	Converged **q**-grid for k @ 300 K
			Atoms in a supercell	**k**-grid	Cutoff[c]		
ALAMODE							
Developer (VASP 6.2.1, ALAMODE 1.3.0)	450	18.3	192/108	2 × 2 × 1/ 2 × 2 × 1	All atoms/ 9nn	0.01/0.03	100 × 100 × 1
Expert (VASP 6.3.0, ALAMODE 1.4.1)	316	40.0	192/192	1 × 1 × 1/ 1 × 1 × 1	All atoms/ 7nn	0.04/0.08	60 × 60 × 1
phono3py							
Expert (VASP 6.2.1, phonopy 2.12.0, phono3py 2.1.0)	600 (H), 550 (C)	21.3	192/108	3 × 3 × 1/ 3 × 3 × 1	All atoms/ all atoms	0.01/0.03	101 × 101 × 1
ShengBTE							
Developer (QE 6.6, ShengBTE 1.2.0)	1388	26.4	DFPT/392	10 × 10 × 1/ 5 × 5 × 1	…/6nn	…/0.01	120 × 120 × 1
Expert (QE 6.7MaX, ShengBTE 1.2.0)	1088	14.3	DFPT/147	12 × 12 × 1/1 × 1 × 1	…/8nn	…/0.01	100 × 100 × 1

[a]In cells where there are two entries separated by a forward slash (/), the first entry corresponds to the harmonic force constants and the second entry corresponds to the cubic force constants.
[b]Unless noted, the same value was used for the harmonic (H) and cubic (C) force constant calculations.
[c]nn, nearest neighbor.

TABLE X. Selected monolayer $MoSe_2$ results.

	a, 2Δ (Å)	Phonon frequency (THz) f_Γ	k @ 300 K [W/(m-K)]	
			k_{pure}	$k_{natural}$
ALAMODE				
Developer	3.270, 3.330	5.03, 7.24, 8.61, 8.74, 10.65	65.1 (RTA)	63.4 (RTA)
Expert	3.269, 3.332	5.01, 7.19, 8.58, 8.70, 10.55	71.5 (RTA)	69.7 (RTA)
phono3py				
Expert	3.270, 3.330	5.03, 7.25, 8.61, 8.74, 10.69	70.5 (RTA), 94.0 (full)	68.1 (RTA), 89.0 (full)
ShengBTE				
Developer	3.267, 3.330	5.04, 7.25, 8.63, 8.76, 10.66	73.8 (RTA), 94.9 (full)	71.0 (RTA), 89.9 (full)
Expert	3.269, 3.328	5.05, 7.25, 8.63, 8.77, 10.65	67.6 (RTA), 88.6 (full)	65.5 (RTA), 84.1 (full)
Experiment[44]				59 ± 18

TABLE XI. Monolayer $MoSe_2$ results related to the long-range Coulombic calculations.

	Cross-plane system size (Å)	Dielectric constant		Born effective charge (e)	
		In-plane	Cross-plane	Mo xy, z	Se xy, z
ALAMODE					
Developer	18.3	6.37	1.44	−1.868, −0.158	0.934, 0.079
Expert	40.0	3.46	1.16	−1.867, −0.122	0.934, 0.061
phono3py					
Expert	21.3	5.62	1.35	−1.868, −0.150	0.934, 0.075
ShengBTE					
Developer	26.4	4.18	1.27	−1.870, −0.137	0.935, 0.069
Expert	14.3	7.90	1.64	−1.893, −0.200	0.946, 0.100

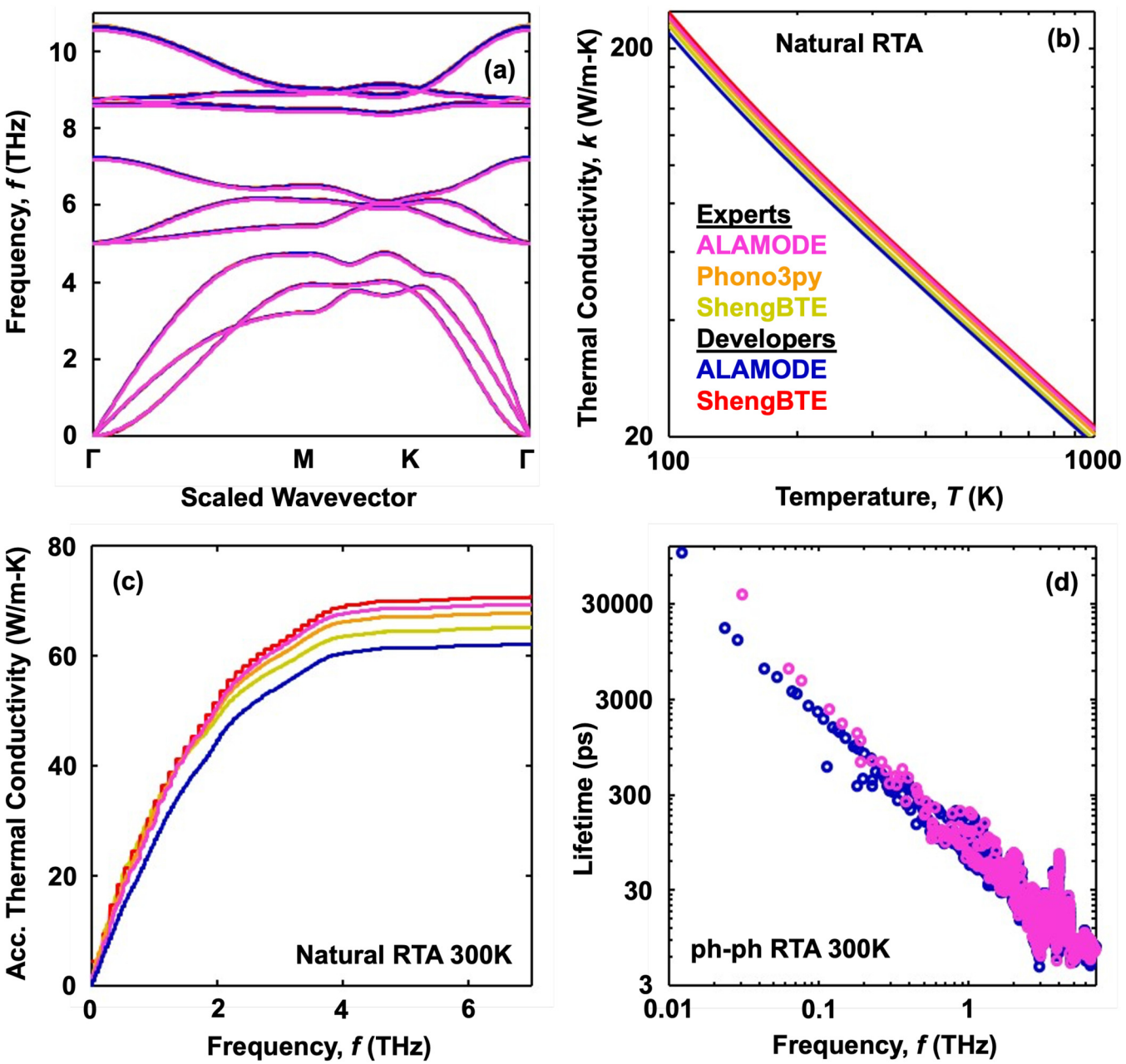

FIG. 9. $MoSe_2$ results. (a) Dispersion. (b) Naturally occurring RTA thermal conductivity. (c) Frequency-dependent thermal conductivity accumulation at 300 K. (d) ALAMODE three-phonon scattering lifetimes at 300 K.

The 300 K in-plane accumulation functions up to a frequency of 5 Thz are plotted in Fig. 10(c). Differences become apparent at frequencies below 1 THz, with the phono3py values increasing slower than those of the other calculations, which is reflected in the three-phonon lifetimes plotted in Fig. 10(d). When comparing how the cubic force constants were calculated by the three teams, there are differences in the supercell size, the **k**-grid, and the cutoff.

E. q-grid convergence

We now consider the convergence of thermal conductivity with the **q**-grid, which is a critical step in the workflow. While

TABLE XII. Comparison of AlN calculation decisions.

	Energy cutoff (eV)[b]	Force constants (harmonic/cubic)[a]			Displacement (Å)	Converged **q**-grid for k @ 300 K[d]
		Atoms in a supercell	**k**-grid	Cutoff[c]		
ALAMODE Collaborative (VASP 6.3.1, ALAMODE 1.4.2)	550	192/192	3×/3×	All atoms/ 15nn	0.01/0.03	53 × 53 × 33
phono3py Collaborative (VASP 6.2.1, phonopy 2.12.0, phono3py 2.1.0)	500	300/72	3×/3 × 3 × 2	All atoms/all atoms	0.03/0.03	31 × 31 × 17
ShengBTE Collaborative (QE 6.7MaX, ShengBTE 1.4.0)	1633	DFPT/300	12×/1×	…/7nn	…/0.01	45×

[a]In cells where there are two entries separated by a forward slash (/), the first entry corresponds to the harmonic force constants and the second entry corresponds to the cubic force constants.
[b]Unless noted, the same value was used for the harmonic (H) and cubic (C) force constant calculations.
[c]nn, nearest neighbor.
[d]None of the teams obtained a converged thermal conductivity at a temperature of 20 K.

specific guidance beyond "Evidence of converged thermal conductivity with varying integration meshes" was not requested from the teams, data were provided in many cases. The available results at 300 K are plotted in Figs. 11(a)–11(d).

In the Ge Free Phase calculations, no quantitative guideline was provided for how well to converge the thermal conductivity with the **q**-grid. For all subsequent calculations, the teams were asked to converge to within a less than 2% difference between successive **q**-grids. In their convergence studies, the teams (i) typically converged to within a difference much smaller than 2% between successive **q**-grids; (ii) started with a **q**-grid as small as 4× and as large as 87×; and (iii) applied spacings between successive **q**-grids that varied between 2 and 30 within the same material and/or for different materials. In a future benchmarking study, it would be wise to provide more guidance on the **q**-grid convergence.

In considering the data in Figs. 11(a)–11(d), thermal conductivity generally increases with a finer **q**-grid. It sometimes decreases, as seen in the phono3py Expert and ShengBTE Expert calculations for RbBr, where those two teams started at coarser grids than the other teams. All of the AlN calculations show some

TABLE XIII. Selected AlN results.

	a, c (Å), u	Phonon frequency (THz)[a,b]			k @ 300 K [W/(m-K)]	
		$f_{\Gamma}(\rightarrow \mathbf{M})$	$f_{\Gamma}(\rightarrow \mathbf{A})$	$f_{\mathbf{A}}$	$k_{in-plane}$	$k_{cross-plane}$
ALAMODE Team	3.114, 4.983, 0.382	18.25, 26.87	19.96, 26.11	5.16, 10.32, 19.77, 24.45	282 (RTA)	263 (RTA)
phono3py Team	3.113, 4.982, 0.381	18.26, 26.88	19.97, 26.12	5.16, 10.32, 19.78, 24.46	253 (RTA), 285 (full)	232 (RTA), 271 (full)
ShengBTE Team	3.116, 4.987, 0.382	18.27, 26.88	19.97, 26.12	5.16, 10.31, 19.78, 24.45	271 (RTA), 298 (full)	251 (RTA), 291 (full)
Experiment[45,72,73]	3.112–3.124, 4.980–4.996, −(291–1073 K)	18.91, 20.04, 22.18, 27.44		5.36, 10.16, –, 25.41		316

[a]The direction-dependent **Γ**-point frequencies correspond to locations of optic phonon splitting. This distinction is not possible in the experimental frequencies. The listed experimental values are those that fall in the same range as those from the calculations.
[b]No temperature was reported in Ref. 73 for the experimental frequencies.

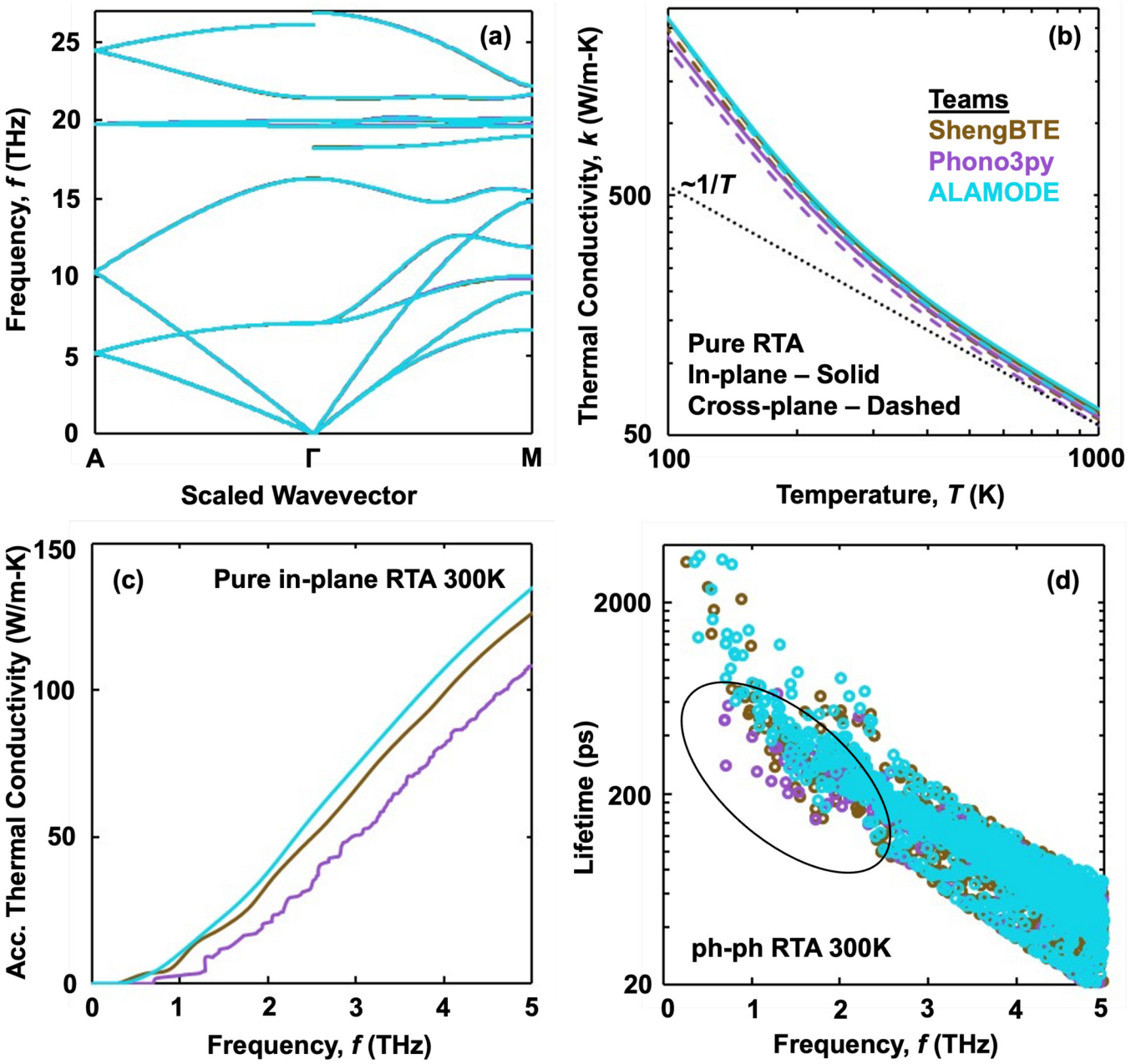

FIG. 10. AlN results. (a) Dispersion. (b) RTA thermal conductivity. (c) Frequency-dependent in-plane thermal conductivity accumulation at 300 K. (d) Phonon–phonon scattering lifetimes at a temperature of 300 K.

oscillation in thermal conductivity with the **q**-grid, most notably for ShengBTE. For a given material, the relative order of the thermal conductivities generally does not change with the **q**-grid (i.e., the curves do not cross), indicating that differences between the calculations are consistent. RbBr, the material with the lowest thermal conductivity, converges the fastest, while monolayer $MoSe_2$ converges the slowest. Generally speaking, one would expect faster convergence for materials where phonons from the full phonon spectrum contribute to thermal conductivity. Slower convergence is expected when low-frequency acoustic phonons dominate thermal conductivity, as these modes are sparsely sampled on a **q**-grid with uniform spacing, as was used in all the calculations.

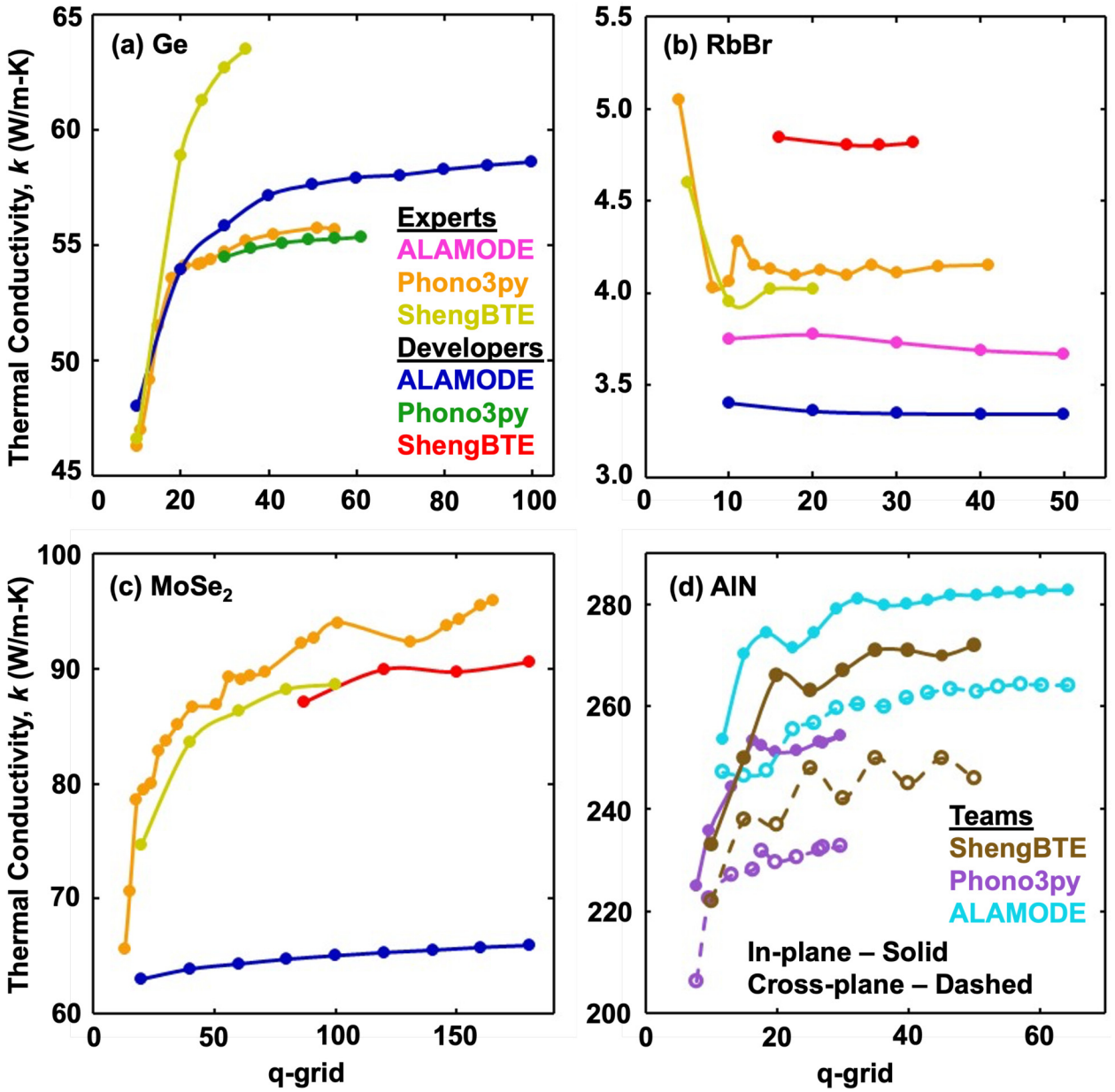

FIG. 11. 300 K thermal conductivity convergence as a function of the **q**-grid for (a) Ge, (b) RbBr, (c) $MoSe_2$, and (d) AlN. In the ALAMODE and phono3py AlN calculations, the **q**-grid resolution was different for the in-plane directions and the cross-plane direction. The plotted **q**-grid corresponds to the average value. All other calculations used an equal **q**-grid in all directions. The ShengBTE Developer calculations were done with naturally occurring isotopes and the full PBTE solution. The ShengBTE Expert calculations were done for the isotopically pure materials and the full PBTE solution. The ALAMODE Developer and Expert calculations were done with naturally occurring isotopes and the RTA. The phono3py Developer and Expert calculations were done for the isotopically pure materials and the full PBTE solution. All AlN calculations were done with the RTA.

For calculations that employ Gaussian functions to ensure energy conservation in the phonon–phonon and phonon-isotope scattering events, the choice of the smearing width affects the thermal conductivity and its **q**-grid convergence. The phono3py Expert calculations for isotopically pure Ge at 300 K from the full PBTE solution are plotted in Fig. 12, showing the convergence for four choices of the smearing width. Also plotted are results from the tetrahedron

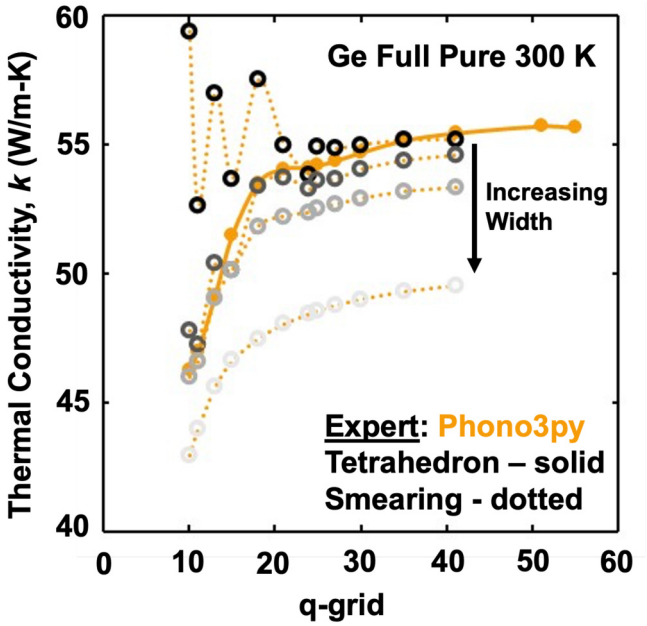

FIG. 12. **q**-grid convergence of the full PBTE solution thermal conductivity of isotopically pure Ge at 300 K from the phono3py Expert calculations. The solid orange curve is from the tetrahedron method, while the dashed curves are from the smearing method with increasing smearing width going from black to light gray circles: 0.01, 0.05, 0.1, and 0.3 THz.

method, which does not require smearing. While the smallest smearing width of 0.01 THz provides a similar converged thermal conductivity as that from the tetrahedron method [55 W/(m-K)], the largest smearing width of 0.3 THz results in a 10% lower thermal conductivity.

Based on the above discussion, we suggest two explanations for the ranges of converged **q**-grids reported by the teams in Tables IV, VII, IX, and XII. First, the non-consistent criteria used by the teams to identify convergence. Second, that earlier decisions in the workflow (e.g., **k**-grid, supercell size, neighbors considered, atomic displacement, and smearing parameter) change the **q**-grid at which convergence is obtained.

VII. CALCULATIONS RELATIVE TO EXPERIMENTS

A. Overview

The main objective of this study is to compare lattice thermal conductivity calculations from three open-source packages. We now provide a brief comparison of the calculations to experimental data for Ge, RbBr, and AlN, where reliable measurements are available (see Tables V, VIII, and XIII).

B. Germanium

The full PBTE solution thermal conductivities at a temperature of 300 K for Ge are all lower than the measured data. For isotopically pure Ge, the calculations range from 55.1 to 64.0 W/(m-K), while the experimental value is 73 W/(m-K) for ^{70}Ge. For naturally occurring Ge, the calculations range from 44.4 to 54.3 W/(m-K), while the experimental value is 62 W/(m-K). If all aspects of the calculations were physically accurate and fully converged, then the resulting thermal conductivities should, in principle, be higher than the corresponding experimental measurements as (i) there are resistive phonon scattering mechanisms that are ignored and (ii) other thermal transport channels (e.g., from electrons) are expected to be negligible. Higher-order phonon–phonon scattering, phonon-defect scattering, and phonon-boundary scattering will all decrease the calculated lattice thermal conductivity. This effect is opposite to what would be required to bring the calculations into better agreement with experiment.

Materials typically expand with increasing temperature, most often leading to softer, lower-frequency phonons. This effect is not considered in the zero-temperature calculation of the phonons used in this study. Phonon softening typically lowers thermal conductivity and would, thus, further exacerbate the discrepancies between measurements and calculations for Ge.

The discrepancies between the calculations and experimental measurements for Ge suggests that DFT (here, at the PBE GGA level) provides limited accuracy in describing the potential energy landscape. For example, the PBEsol GGA exchange-correlation functional for Ge is too soft, leading to a larger lattice constant and phonon softening compared to the experiments (Table V). Lower phonon frequencies tend to lower the phonon group velocities, one factor that may explain the lower thermal conductivities compared to the experiments. At the local density approximation (LDA) level of DFT with zero-temperature phonons and three-phonon scattering, Lindsay *et al.* calculated the 300 K thermal conductivity of Ge to be 74 W/m K (isotopically pure) and 60 W/m K (naturally occurring) from a full solution of the PBTE.[67] These values, which are larger than any calculated here, are consistent with the LDA exchange-correlation functional being stiffer than those at the GGA level.

Previous studies have investigated the effect of the exchange-correlation functional on the phonon properties and thermal conductivity of silicon,[74,75] graphene,[76,77] AlAs and BAs,[78] and a series of rock salt and zinc blende semiconductors.[79] The calculated thermal conductivities fall above and below experimental measurements. These results indicate that deficiencies in the phonon transport theory are not sufficient to explain discrepancies compared to measurements, supporting our conclusion of the role played by the DFT calculations.

C. RbBr

The full PBTE solution calculations of the thermal conductivity of naturally occurring RbBr at 300 K (3.92–4.80 W/m K) overestimate measured values at room temperature (3.2–3.4 W/m K).[42,43] Given the above discussion for Ge, this overestimation may seem surprising, given that the calculated lattice parameters are 2% larger than the experiments and the highest optic Raman-active frequencies are 10% lower than the experiments. Extrinsic scattering mechanisms (e.g., point defects and grain boundaries) are possible causes for such discrepancies. The sample descriptions in these experimental studies, however, do not suggest that crystal quality

was providing significant thermal resistance. We also note that the thermal conductivity measurements on single-crystal[42] and polycrystalline samples[43] produced similar values. The model fittings and analysis of the measured temperature-dependent thermal conductivity for RbBr in Ref. 42 suggest that four-phonon scattering processes may be important, even at room temperature. Further analysis would be required to fully understand the discrepancy between the calculated and measured thermal conductivities.

Chang *et al.* calculated the phonon properties and thermal conductivity of RbBr at the LDA level of DFT with zero-temperature phonons and three-phonon scattering.[80] Compared to the GGA results presented here, they found a smaller lattice constant of 6.70 Å, a larger maximum **Γ**-point frequency of 4 THz, and a larger 300 K full PBTE solution thermal conductivity of 6 W/(m-K), which is almost double the experimental measurement. These effects of LDA vs GGA are consistent with those noted above for Ge.

D. AlN

The calculated full PBTE solution AlN cross-plane thermal conductivity values, 271 and 291 W/(m-K), underestimate the measurement[45] of 316 W/(m-K) by 8%–14%. This underestimation is smaller than the 12%–25% underestimation for Ge. As with Ge, the calculated phonon frequencies are underestimated, although to a lesser degree: 2%–4% for AlN vs 4%–7% for Ge. The AlN calculated lattice constants are within 0.1% of the measurements, compared to the Ge values, which are within 0.5%–0.8%. As a stiffer material than Ge, smaller differences in AlN's lattice constants can lead to relatively larger differences in the force constants and phonon properties.

Others have calculated the cross-plane thermal conductivity of AlN at 300 K using the full solution of the PBTE and different choices related to the DFT and lattice dynamics calculations. Lindsay *et al.*[67] and Li and Mingo[81] studied AlN at the LDA level using zero-temperature phonons and three-phonon scattering. They found thermal conductivities of 322 and ∼300 W/(m-K). These values are comparable to the experimental measurement[45] of 316 W/(m-K) and are higher than all the results obtained here at the PBE GGA level. Shulumba *et al.* found that phonon renormalization was not important in AlN at 300 K.[82] They reported a thermal conductivity of 320 W/(m-K) based on DFT calculations at the PBE GGA level and three-phonon scattering, which is comparable to the previous LDA results. Wang *et al.* included four-phonon scattering in AlN modeled at the PBE GGA level and found a thermal conductivity of 268 W/(m-K).[83] They reported that including four-phonon scattering reduced the thermal conductivity at 800 K by 13% and that the effect was smaller at lower temperatures.

VIII. RECOMMENDATIONS FOR BEST PRACTICES

A. Code version

The most up-to-date versions of the DFT and transport packages should typically be used. When comparing to published results that used earlier versions, however, it may not be possible to obtain an agreement. When publishing work, it is essential to specify the code versions used and provide input files that can be used to repeat the calculations.

Changes were made to some of the packages as a result of this work. For example, a bug was corrected in ALAMODE (present in versions before 1.4.2) related to the calculation of some phonon velocities when implementing non-analytic long-range Coulombic corrections via the Ewald sum approach.[84] This bug was not an issue for long-range corrections using the mixed-space method[47] within ALAMODE.

Another example of a change was in phono3py (before version 3.0) and ALAMODE (before version 1.5.0). In these versions, the cubic force constants violated particular symmetries when (i) no neighbor cutoff distance was specified (i.e., using all atoms in the supercell) or (ii) the neighbor cutoff distance was more than half of the supercell size. This violation led to an overestimation of the low-frequency scattering rates and thus an underestimation of thermal conductivity (see Sec. V B). This issue is resolved in the later versions of these packages.

B. Convergence

Convergence tests at all stages of the workflow are integral to any calculation of phonon properties and thermal conductivity. Many of the required choices are not independent (e.g., the smearing widths for the phonon scattering events and the **q**-grid for integrating over the Brillouin zone, as shown in Fig. 12 for Ge). It is computationally infeasible, however, to perform a multi-dimensional convergence study that includes all the decisions related to the DFT, structure, harmonic, anharmonic, and thermal conductivity calculations. An interesting direction for future work would be to develop an efficient and rigorous approach for establishing convergence. Careful convergence testing can also help to quantify uncertainty, an area where the majority of reported work is lacking.

A thorough literature review for the material to be studied, or related materials, can provide a starting point for the computational decisions. Significant work has been done for specifying DFT parameters, such as thresholds, energy cutoffs, and **k**-grids for lattice constant calculations for many materials. The checklists for the materials in this study can also serve as guidance for a new material.

For displacement-based calculations of harmonic and cubic force constants, the key convergence-related decisions are the supercell size and the associated **k**-grid, the number of neighbors considered (i.e., the cutoff), and size of the atomic displacement; for example, small supercells can lead to unwanted images in the periodic DFT simulations and too small of a cutoff can neglect important interactions.

The **q**-grid should be chosen to ensure a converged thermal conductivity for each studied condition [Figs. 11(a)–11(d)]. For example, a **q**-grid that provides convergence at one temperature may not be sufficient to achieve convergence at lower temperatures due to the increasing importance of low-frequency modes as dictated by Bose–Einstein statistics.[85] As noted in Table XII, challenges were observed in the AlN thermal conductivity calculations at a temperature of 20 K, where none of the teams were able to identify a converged **q**-grid. Related to this point, evenly spaced **q**-grids, as used in the three packages studied here, undersample low-frequency modes relative to high-frequency modes.

We also note that because thermal conductivity [Eq. (1)] is integrated over all modes in the Brillouin zone, numerical inaccuracies in the mode-resolved lifetimes may cancel and **q**-grid convergence may be easier to achieve than convergence of the lifetimes. The lifetimes themselves are determined by sums of scattering processes. The interplay of the **q**-grid size with the implementation of energy and momentum conservation conditions, however, can be strongly non-linear. At low temperatures, where only a small number of modes are thermally populated, accurately determining their converged lifetimes may be required to obtain a truly converged thermal conductivity. In a future benchmarking study, it would be valuable to compare lifetimes from different teams obtained from the same **q**-grid.

C. Accuracy

The required accuracy of a thermal conductivity calculation depends on the user's needs and constraints (e.g., computational time). The primary driver for the thermal conductivity variations reported here is the calculation of the cubic force constants. In most cases, differences in the phonon dispersions, which are calculated at the harmonic level, were negligible.

If the objective of a study is to best match experimental measurements, as is often the case, then there are important decisions to be made in the structural and harmonic calculations. Specifically, the pseudopotential and exchange-correlation functional should be chosen so as to best match measured lattice constants and phonon dispersion data. If the structure and phonons cannot be matched, then there cannot be confidence in further calculations of thermal conductivity. At this stage, it is also important to ensure that there are no imaginary phonon modes, which can be a sign of the need for stricter DFT parameters (e.g., **k**-grid sampling) or a dynamic instability of a low-temperature structure.

When examining thermal conductivity variations with isotopic mass disorder, the single atomic mass that must be specified for the dispersion and phonon–phonon scattering calculations should be carefully considered. This mass directly affects the phonon frequencies, and thus the intrinsic thermal conductivity, via variations in the phase space for phonon–phonon scattering. We found, for example, that one set of isotopically pure Ge calculations using a mass of 69.924 amu gave a 300 K thermal conductivity that was 2% higher than when using the isotopically averaged mass of 72.640 amu.

The additional decisions required in more advanced calculations can also affect the thermal conductivity. For example, Li *et al.* found that the sequence of calculating temperature-dependent harmonic and higher-order force constants (e.g., all-at-once or sequentially) affects the thermal conductivity of Tl_3VSe_4.[86] Zhou *et al.* found that the energy surface roughness in a DFT calculation can lead to an underestimation of thermal conductivity unless sufficiently large atomic displacements are used to calculate the quartic force constants.[87]

IX. SUMMARY AND OUTLOOK

This study provided a benchmark of three commonly used, open-source software packages (ALAMODE, phono3py, and ShengBTE; Sec. IV A) for calculating phonon properties and thermal conductivity in crystalline materials using lattice dynamics techniques and a solution of the PBTE. Though having different numerical implementations, each package is based on the same underlying theories and can be coupled with DFT calculations of atomic interactions. The phonons were determined at zero temperature. Lowest-order anharmonic perturbation theory was used to describe three-phonon interactions. Phonon scattering from randomly distributed isotopes was also considered. From this starting point, the calculations can be compared with each other and serve as a foundation for including higher levels of theory.

The calculations were carried out by the developers and expert users of each package (Sec. IV B). Four relatively simple insulating materials (Ge, RbBr, monolayer $MoSe_2$, and AlN; Sec. III) that covered a range of room temperature thermal conductivities (3–300 W/m K) were considered. Calculated phonon dispersions, temperature-dependent thermal conductivities, 300 K thermal conductivity accumulations, and 300 K lifetimes were compared and contrasted for each material in Secs. V and VI. The most significant effort was spent examining Ge to understand how the developers and experts applied the packages and to gain insights into variations among the calculations.

All three packages provided similar thermal conductivity results for all the materials, with variations within $\pm 15\%$ of the mean values over a wide range of temperatures. In particular, when using the same input harmonic and cubic force constants for Ge, the RTA thermal conductivity variations among the packages are less than 1% (Sec. V B). In general, the calculated thermal conductivities do not show good agreement with experimental measurements (Sec. VII), which we attributed to limitations in the DFT calculations used to describe the atomic interactions.

For all materials, variations in thermal conductivities were found to most likely derive from the calculation of the cubic force constants and their post-processing (i.e., application of symmetries). In ALAMODE, we note that the translational invariance and symmetry constraints are incorporated during the fitting process. These calculations depend on a variety of choices, including the supercell size, neighbor interaction cutoff, atomic displacement, and symmetry enforcement. The cutoff, in particular, can have a large effect, as shown in Figs. 2(b), 5(b), and 6(b). Due to their complex interplay, no obvious correlations were observed between these choices and the resulting thermal conductivities. Recommendations for best practices as related to code version, convergence, and accuracy were provided in Sec. VIII. More systematic studies than what was carried out here would be required to determine the underlying origin(s) of the differences. A future benchmark study that includes additional packages and examines materials with greater complexity also has the potential to provide deeper insights.

Significant developments continue to be realized in the theoretical and numerical description of lattice thermal conductivity beyond the zero-temperature phonons that interact through the three-phonon and phonon-isotope scattering processes that were studied here. These include renormalization (i.e., finite-temperature phonons),[16,22] four-phonon interactions,[23–25] phonon-defect interactions,[26,27] electron-phonon interactions,[31–35] and vibrational transport due phonon coherences.[36–39] Furthermore, the development of machine learning potentials trained on DFT calculations presents an opportunity for decreasing the computational cost and

making calculations on crystals with large unit cells and/or low symmetry more tractable.[19,88–92] As these methodologies become standard practice, benchmark studies similar to that presented here will be essential.

SUPPLEMENTARY MATERIAL

See the supplementary material for the materials checklists, results from the ALAMODE Expert QE calculations, and further details about the Ge cubic force constants presented in Table VI.

ACKNOWLEDGMENTS

The organizers were supported by the National Science Foundation (Award No. DMR-2025013; A.J.H.M.) and the U.S. Department of Energy, Office of Science, Office of Basic Energy Sciences, Materials Sciences and Engineering Division (L.L. and R.J.).

The ALAMODE Developer team (R.M. and T.T.) was supported by JSPS KAKENHI (Grant No. 21K03424), the Grant-in-Aid for Japan Society for the Promotion of Science (JSPS) Fellows (No. 22J20892), and the MEXT Program: Data Creation and Utilization-Type Material Research and Development Project (Digital Transformation Initiative Center for Magnetic Materials) (Grant No. JPMXP1122715503).

The ALAMODE Expert team was supported by CREST (Grant Nos. JPMJCR19I2 and JPMJCR21O2) from the Japan Science and Technology Agency (J.S.), KAKENHI (Grant No. 22H04950) from the JSPS (J.S.), the Quantum Science and Technology Fellowship Program (Q-STEP) from the University of Tokyo (T.H.), the Research Fellowship for Young Scientists DC2 (Grant No. 23KJ0511) from JSPS (T.H.), the Research Fellowship for Young Scientists DC1 (Grant Nos. 21J21731 and 22KJ0648) from JSPS (H.M.), The University of Tokyo Fellowship (H.M.), the Excellent Young Scientists Fund (Overseas) of Shandong Province (Grant No. 2023HWYQ-107) (C.S.), and the Taishan Scholars Program of Shandong Province (C.S.).

The phono3py Developer team (A.T.) was supported by JSPS KAKENHI (Grant Nos. JP21K04632 and JP24K08021). Some of the calculations were performed on the Numerical Materials Simulator at NIMS.

The phono3py Expert team (T.P.) was supported by the Research Foundation Flanders (FWO-Vl) through a senior postdoctoral fellowship.

The ShengBTE Developer team was supported by the Natural Science Foundation of China (Grant No. 12174261) and the GuangDong Basic and Applied Basic Research Foundation (Grant No. 2023A1515010365) (W.L.). This research used, in part, resources on the Palmetto Cluster[93] at Clemson University under National Science Foundation (Awards MRI 1228312, II NEW 1405767, MRI 1725573, and MRI 2018069; F.M.).

The ShengBTE Expert Team (H.B., S.L., A.W., and X.Z.) was supported by the National Natural Science Foundation of China (NSFC) (No. 52122606), the Shanghai Municipal Natural Science Foundation (Grant No. 22YF1400100), and the Fundamental Research Funds for the Central Universities (Grant No. 2232022D-22).

AUTHOR DECLARATIONS

Conflict of Interest

The authors have no conflicts to disclose.

Author Contributions

Alan J. H. McGaughey: Conceptualization (equal); Formal analysis (equal); Funding acquisition (equal); Methodology (equal); Project administration (equal); Supervision (equal); Visualization (equal); Writing – original draft (equal); Writing – review & editing (equal). **Lucas Lindsay:** Conceptualization (equal); Data curation (equal); Formal analysis (equal); Funding acquisition (equal); Methodology (equal); Project administration (equal); Supervision (equal); Visualization (equal); Writing – original draft (equal); Writing – review & editing (equal). **Hua Bao:** Project administration (equal); Resources (equal); Supervision (equal); Writing – review & editing (equal). **Tomu Hamakawa:** Data curation (supporting); Formal analysis (supporting); Investigation (equal); Methodology (equal); Validation (equal); Writing – review & editing (supporting). **Rinkle Juneja:** Data curation (equal); Software (equal); Validation (equal); Writing – review & editing (equal). **Shouhang Li:** Supervision (equal); Validation (equal); Writing – review & editing (equal). **Wu Li:** Funding acquisition (equal); Software (equal); Writing – review & editing (equal). **Ryota Masuki:** Formal analysis (equal); Methodology (equal); Software (equal); Writing – review & editing (equal). **Fanchen Meng:** Data curation (equal); Resources (equal); Writing – review & editing (equal). **Han Meng:** Data curation (supporting); Formal analysis (supporting); Investigation (equal); Methodology (equal); Validation (equal); Writing – review & editing (supporting). **Tribhuwan Pandey:** Data curation (equal); Formal analysis (equal); Investigation (equal); Resources (equal); Software (equal); Validation (equal); Writing – review & editing (equal). **Cheng Shao:** Data curation (equal); Formal analysis (equal); Investigation (equal); Methodology (equal); Software (equal); Validation (equal); Writing – review & editing (supporting). **Junichiro Shiomi:** Conceptualization (equal); Funding acquisition (equal); Project administration (equal); Resources (equal); Supervision (equal); Writing – review & editing (equal). **Terumasa Tadano:** Formal analysis (equal); Methodology (equal); Software (equal); Writing – review & editing (equal). **Atsushi Togo:** Formal analysis (equal); Funding acquisition (equal); Investigation (equal); Software (equal). **Ao Wang:** Data curation (equal); Validation (equal); Writing – review & editing (equal). **Xinyu Zhang:** Data curation (equal); Validation (equal); Writing – review & editing (equal).

DATA AVAILABILITY

Input files required to run the calculations discussed in this paper and comprehensive results from all teams are openly available in GitHub at https://github.com/McGaughey-Lab/Phonon-Olympics, Ref. 57.

REFERENCES

[1]K. Esfarjani, J. Garg, and G. Chen, "Modeling heat conduction from first-principles," Annu. Rev. Heat Transfer **17**, 9–47 (2014).

[2]L. Lindsay, "First principles Peierls-Boltzmann phonon thermal transport: A topical review," Nanoscale Microscale Thermophys. Eng. **20**, 67–84 (2016).
[3]L. Lindsay, C. Hua, X. L. Ruan, and S. Lee, "Survey of *ab initio* phonon thermal transport," Mater. Today Phys. **7**, 106–120 (2018).
[4]A. J. H. McGaughey, A. Jain, H.-Y. Kim, and B. Fu, "Phonon properties and thermal conductivity from first principles, lattice dynamics, and the Boltzmann transport equation," J. Appl. Phys. **125**, 011101 (2019).
[5]T. Tadano, Y. Gohda, and S. Tsuneyuki, "Anharmonic force constants extracted from first-principles molecular dynamics: Applications to heat transfer simulations," J. Phys.: Condens. Matter **26**, 225402 (2014).
[6]A. Togo, L. Chaput, and I. Tanaka, "Distributions of phonon lifetimes in Brillouin zones," Phys. Rev. B **91**, 094306 (2015).
[7]A. Togo, L. Chaput, T. Tadano, and I. Tanaka, "Implementation strategies in phonopy and phono3py," J. Phys.: Condens. Matter **35**, 353001 (2023).
[8]W. Li, J. Carrete, N. A. Katcho, and N. Mingo, "ShengBTE: A solver of the Boltzmann transport equation for phonons," Comput. Phys. Commun. **185**, 1747–1758 (2014).
[9]J. Carrete, B. Vermeersch, A. Katre, A. van Roekeghem, T. Wang, G. K. Madsen, and N. Mingo, "almaBTE: A solver of the space–time dependent Boltzmann transport equation for phonons in structured materials," Comput. Phys. Commun. **220**, 351–362 (2017).
[10]F. Eriksson, E. Fransson, and P. Erhart, "The hiPhive package for the extraction of high-order force constants by machine learning," Adv. Theory Simul. **2**, 1800184 (2019).
[11]F. Zhou, W. Nielson, Y. Xia, V. Ozoliņš *et al.*, "Compressive sensing lattice dynamics. I. General formalism," Phys. Rev. B **100**, 184308 (2019).
[12]G. Barbalinardo, Z. Chen, N. W. Lundgren, and D. Donadio, "Efficient anharmonic lattice dynamics calculations of thermal transport in crystalline and disordered solids," J. Appl. Phys. **128**, 135104 (2020).
[13]L. Monacelli, R. Bianco, M. Cherubini, M. Calandra, I. Errea, and F. Mauri, "The stochastic self-consistent harmonic approximation: Calculating vibrational properties of materials with full quantum and anharmonic effects," J. Phys.: Condens. Matter **33**, 363001 (2021).
[14]N. H. Protik, C. Li, M. Pruneda, D. Broido, and P. Ordejón, "The elphbolt ab initio solver for the coupled electron-phonon Boltzmann transport equations," npj Comput. Mater. **8**, 28 (2022).
[15]A. Cepellotti, J. Coulter, A. Johansson, N. S. Fedorova, and B. Kozinsky, "Phoebe: A high-performance framework for solving phonon and electron Boltzmann transport equations," J. Phys.: Mater. **5**, 035003 (2022).
[16]F. Knoop, N. Shulumba, A. Castellano, J. P. Alvarinhas Batista, R. Farris, M. J. Verstraete, M. Heine, D. Broido, D. S. Kim, J. Klarbring *et al.*, "TDEP: Temperature dependent effective potentials," J. Open Source Softw. **9**, 6150 (2024).
[17]K. Esfarjani, H. Stokes, S. N. Sadeghi, Y. Liang, B. Timalsina, H. Meng, J. Shiomi, B. Liao, and R. Sun, "ALATDYN: A set of Anharmonic LATtice DYNamics codes to compute thermodynamic and thermal transport properties of crystalline solids," Comput. Phys. Commun. **312**, 109575 (2025).
[18]A. Rodriguez, C. Lin, H. Yang, M. Al-Fahdi, C. Shen, K. Choudhary, Y. Zhao, J. Hu, B. Cao, H. Zhang *et al.*, "Million-scale data integrated deep neural network for phonon properties of heuslers spanning the periodic table," npj Comput. Mater. **9**, 20 (2023).
[19]J. Li, Z. Chen, Q. Wang, H. Yang, Z. Lu, G. Li, S. Chen, Y. Zhu, X. Liu, J. Tan *et al.*, "Probing the limit of heat transfer in inorganic crystals with deep learning," arXiv:2503.11568 (2025).
[20]M. Ohnishi, T. Deng, P. Torres, Z. Xu, T. Tadano, H. Zhang, W. Nong, M. Hanai, Z. Tian, M. Hu *et al.*, "Database and deep-learning scalability of anharmonic phonon properties by automated brute-force first-principles calculations," arXiv:2504.21245 (2025).
[21]A. Jain, Y. Srivastava, A. G. Gokhale, N. Virakante, and H. L. Kagdada, "Higher-order thermal transport theory for phonon thermal transport in semiconductors using lattice dynamics calculations and the boltzmann transport equation," arXiv:2505.23307 (2025).
[22]N. K. Ravichandran and D. Broido, "Unified first-principles theory of thermal properties of insulators," Phys. Rev. B **98**, 085205 (2018).
[23]T. Feng and X. Ruan, "Quantum mechanical prediction of four-phonon scattering rates and reduced thermal conductivity of solids," Phys. Rev. B **93**, 045202 (2016).
[24]T. Feng, L. Lindsay, and X. Ruan, "Four-phonon scattering significantly reduces intrinsic thermal conductivity of solids," Phys. Rev. B **96**, 161201 (2017).
[25]Y. Xia, "Revisiting lattice thermal transport in PbTe: The crucial role of quartic anharmonicity," Appl. Phys. Lett. **113**, 073901 (2018).
[26]N. A. Katcho, J. Carrete, W. Li, and N. Mingo, "Effect of nitrogen and vacancy defects on the thermal conductivity of diamond: An *ab initio* Green's function approach," Phys. Rev. B **90**, 094117 (2014).
[27]C. A. Polanco and L. Lindsay, "Thermal conductivity of InN with point defects from first principles," Phys. Rev. B **98**, 014306 (2018).
[28]A. J. H. McGaughey, E. S. Landry, D. P. Sellan, and C. H. Amon, "Size-dependent model for thin film and nanowire thermal conductivity," Appl. Phys. Lett. **99**, 131904 (2011).
[29]A. Jain, Y.-J. Yu, and A. J. H. McGaughey, "Phonon transport in periodic silicon nanoporous films with feature sizes greater than 100 nm," Phys. Rev. B **87**, 195301 (2013).
[30]T. Hori, J. Shiomi, and C. Dames, "Effective phonon mean free path in polycrystalline nanostructures," Appl. Phys. Lett. **106**, 171901 (2015).
[31]S. Poncé, E. R. Margine, C. Verdi, and F. Giustino, "EPW: Electron–phonon coupling, transport and superconducting properties using maximally localized Wannier functions," Comput. Phys. Commun. **209**, 116–133 (2016).
[32]A. Jain and A. J. H. McGaughey, "Thermal transport by phonons and electrons in aluminum, silver, and gold from first principles," Phys. Rev. B **93**, 081206 (2016).
[33]C. Li, N. K. Ravichandran, L. Lindsay, and D. Broido, "Fermi surface nesting and phonon frequency gap drive anomalous thermal transport," Phys. Rev. Lett. **121**, 175901 (2018).
[34]Y. Chen, J. Ma, and W. Li, "Understanding the thermal conductivity and Lorenz number in tungsten from first principles," Phys. Rev. B **99**, 020305 (2019).
[35]Z. Tong, S. Li, X. Ruan, and H. Bao, "Comprehensive first-principles analysis of phonon thermal conductivity and electron-phonon coupling in different metals," Phys. Rev. B **100**, 144306 (2019).
[36]M. Simoncelli, N. Marzari, and F. Mauri, "Unified theory of thermal transport in crystals and glasses," Nat. Phys. **15**, 809–813 (2019).
[37]M. Simoncelli, N. Marzari, and F. Mauri, "Wigner formulation of thermal transport in solids," Phys. Rev. X **12**, 041011 (2022).
[38]J. Yang, A. Jain, and W.-L. Ong, "Inter-channel conversion between population-/coherence-channel dictates thermal transport in $MAPbI_3$ crystals," Mater. Today Phys. **28**, 100892 (2022).
[39]L. Isaeva, G. Barbalinardo, D. Donadio, and S. Baroni, "Modeling heat transport in crystals and glasses from a unified lattice-dynamical approach," Nat. Commun. **10**, 3853 (2019).
[40]S. Tamura, "Isotope scattering of dispersive phonons in Ge," Phys. Rev. B **27**, 858–866 (1983).
[41]V. Ozhogin, A. Inyushkin, A. Taldenkov, A. Tikhomirov, G. Popov, E. Haller, and K. Itoh, "Isotope effect in the thermal conductivity of germanium single crystals," J. Exp. Theor. Phys. Lett. **63**, 490–494 (1996).
[42]J. P. Moore, R. K. Williams, and R. S. Graves, "Lattice thermal conductivities of RbBr, RbI, and RbCl from 80 to 400 K," Phys. Rev. B **11**, 3107 (1975).
[43]P. Andersson, "Thermal conductivity under pressure and through phase transitions in solid alkali halides. I. Experimental results for KCl, KBr, KI, RbCl, RbBr and RbI," J. Phys. C: Solid State Phys. **18**, 3943 (1985).
[44]X. Zhang, D. Sun, Y. Li, G.-H. Lee, X. Cui, D. Chenet, Y. You, T. F. Heinz, and J. C. Hone, "Measurement of lateral and interfacial thermal conductivity of single-and bilayer MoS_2 and $MoSe_2$ using refined optothermal Raman technique," ACS Appl. Mater. Interfaces **7**, 25923–25929 (2015).
[45]A. Inyushkin, A. Taldenkov, D. Chernodubov, E. Mokhov, S. Nagalyuk, V. Ralchenko, and A. Khomich, "On the thermal conductivity of single crystal AlN," J. Appl. Phys. **127**, 205109 (2020).

[46]P. Giannozzi, S. de Gironcoli, P. Pavone, and S. Baroni, "*Ab initio* calculation of phonon dispersions in semiconductors," Phys. Rev. B **43**, 7231–7242 (1991).
[47]Y. Wang, J. Wang, W. Wang, Z. Mei, S. Shang, L. Chen, and Z. Liu, "A mixed-space approach to first-principles calculations of phonon frequencies for polar materials," J. Phys.: Condens. Matter **22**, 202201 (2010).
[48]J. Carrete, W. Li, L. Lindsay, D. A. Broido, L. J. Gallego, and N. Mingo, "Physically founded phonon dispersions of few-layer materials and the case of borophene," Mater. Res. Lett. **4**, 204–211 (2016).
[49]N. Bonini, J. Garg, and N. Marzari, "Acoustic phonon lifetimes and thermal transport in free-standing and strained graphene," Nano Lett. **12**, 2673–2678 (2012).
[50]L. Lindsay, W. Li, J. Carrete, N. Mingo, D. Broido, and T. Reinecke, "Phonon thermal transport in strained and unstrained graphene from first principles," Phys. Rev. B **89**, 155426 (2014).
[51]P. E. Blöchl, O. Jepsen, and O. K. Andersen, "Improved tetrahedron method for Brillouin-zone integrations," Phys. Rev. B **49**, 16223 (1994).
[52]P. Giannozzi, S. Baroni, N. Bonini, M. Calandra, R. Car, C. Cavazzoni, D. Ceresoli, G. L. Chiarotti, M. Cococcioni, I. Dabo, A. D. Corso, S. de Gironcoli, S. Fabris, G. Fratesi, R. Gebauer, U. Gerstmann, C. Gougoussis, A. Kokalj, M. Lazzeri, L. Martin-Samos, N. Marzari, F. Mauri, R. Mazzarello, S. Paolini, A. Pasquarello, L. Paulatto, C. Sbraccia, S. Scandolo, G. Sclauzero, A. P. Seitsonen, A. Smogunov, P. Umari, and R. M. Wentzcovitch, "QUANTUM ESPRESSO: A modular and open-source software project for quantum simulations of materials," J. Phys.: Condens. Matter **21**, 395502 (2009).
[53]P. Giannozzi, O. Andreussi, T. Brumme, O. Bunau, M. B. Nardelli, M. Calandra, R. Car, C. Cavazzoni, D. Ceresoli, M. Cococcioni *et al.*, "Advanced capabilities for materials modelling with Quantum Espresso," J. Phys.: Condens. Matter **29**, 465901 (2017).
[54]G. Kresse and J. Hafner, "*Ab initio* molecular dynamics for liquid-metals," Phys. Rev. B **47**, 558–561 (1993).
[55]G. Kresse and J. Furthmuller, "Efficient iterative schemes for *ab initio* total-energy calculations using a plane-wave basis set," Phys. Rev. B **54**, 11169–11186 (1996).
[56]G. Kresse and J. Furthmuller, "Efficiency of ab-initio total energy calculations for metals and semiconductors using a plane-wave basis set," Comput. Mater. Sci. **6**, 15–50 (1996).
[57]"McGaughey-Lab/Phonon-Olympics," Github, available at https://github.com/McGaughey-Lab/Phonon-Olympics (2025).
[58]G. Nilsson and G. Nelin, "Study of the homology between silicon and germanium by thermal-neutron spectrometry," Phys. Rev. B **6**, 3777–3786 (1972).
[59]M. Hu, H. Sinn, A. Alatas, W. Sturhahn, E. Alp, H.-C. Wille, Y. V. Shvyd'ko, J. Sutter, J. Bandaru, E. Haller *et al.*, "Effect of isotopic composition on the lattice parameter of germanium measured by x-ray backscattering," Phys. Rev. B **67**, 113306 (2003).
[60]R. A. Guyer and J. A. Krumhansl, "Thermal conductivity, second sound, and phonon hydrodynamic phenomena in nonmetallic crystals," Phys. Rev. **148**, 778–788 (1966).
[61]A. Cepellotti, G. Fugallo, L. Paulatto, M. Lazzeri, F. Mauri, and N. Marzari, "Phonon hydrodynamics in two-dimensional materials," Nat. Commun. **6**, 6400 (2015).
[62]T. Kawabata, K. Shimura, Y. Ishii, M. Koike, K. Yoshida, S. Yonehara, K. Yokoi, A. Subedi, K. Behnia, and Y. Machida, "Phonon hydrodynamic regimes in sapphire," Phys. Rev. Res. **7**, 033017 (2025).
[63]This difference arose because some periodic supercell images for the all-neighbor calculations have the same distance from the central atom, which introduces ambiguity in constructing the phase factors that enter the scattering rates. For cutoff distances confining interactions within the supercell, e.g., third nearest neighbors here, there is no ambiguity. To work around this, ALAMODE and phono3py calculated each possibility and averaged the rates. This approach, however, breaks the wave vector permutation symmetry and is a likely cause of the decreased thermal conductivity for the all-neighbor calculation. The codes have since been modified to maintain wave vector permutation symmetry, leading to results that are similar to those for the third nearest neighbor calculations.
[64]Phono3py implements Eq. (12) from Ref. 40, where the frequency of the mode being scattered appears to the second power, outside of the summation over all other modes. In the ALAMODE implementation of Eq. (12) from Ref. 40, the frequency of the mode being scattered appears to the first power outside of the summation and the frequency of the other mode appears inside the summation. Due to the assumption of elastic scattering, these two frequencies must be the same. In practice, however, due to the finite number of modes considered in the calculations and required mode broadening, there may be small differences between these two approaches.
[65]P. Haas, F. Tran, and P. Blaha, "Calculation of the lattice constant of solids with semilocal functionals," Phys. Rev. B **79**, 085104 (2009).
[66]T. Tadano and S. Tsuneyuki, "First-principles lattice dynamics method for strongly anharmonic crystals," J. Phys. Soc. Jpn. **87**, 041015 (2018).
[67]L. Lindsay, D. A. Broido, and T. L. Reinecke, "*Ab initio* thermal transport in compound semiconductors," Phys. Rev. B **87**, 165201 (2013).
[68]H. Xie, X. Gu, and H. Bao, "Effect of the accuracy of interatomic force constants on the prediction of lattice thermal conductivity," Comput. Mater. Sci. **138**, 368–376 (2017).
[69]V. T. Deshpande and D. B. Sirdeshmukh, "Thermal expansion of ammonium bromide, rubidium bromide and rubidium chloride," Acta Crystallogr. **14**, 353–355 (1961).
[70]S. Rolandson and G. Raunio, "Lattice dynamics of RbBr," J. Phys. C: Solid State Phys. **4**, 958 (1971).
[71]A. Laturia, M. L. Van de Put, and W. G. Vandenberghe, "Dielectric properties of hexagonal boron nitride and transition metal dichalcogenides: From monolayer to bulk," npj 2D Mater. Appl. **2**, 6 (2018).
[72]W. M. Yim and R. J. Paff, "Thermal expansion of AlN, sapphire, and silicon," J. Appl. Phys. **45**, 1456–1457 (1974).
[73]M. Schwoerer-Böhning, A. Macrander, M. Pabst, and P. Pavone, "Phonons in wurtzite aluminum nitride," Phys. Status Solidi B **215**, 177–180 (1999).
[74]A. Jain and A. J. H. McGaughey, "Effect of exchange–correlation on first-principles-driven lattice thermal conductivity predictions of crystalline silicon," Comput. Mater. Sci. **110**, 115–120 (2015).
[75]H. L. Parks, H.-Y. Kim, V. Viswanathan, and A. J. H. McGaughey, "Uncertainty quantification in first-principles predictions of phonon properties and lattice thermal conductivity," Phys. Rev. Mater. **4**, 083805 (2020).
[76]G. Qin, Z. Qin, H. Wang, and M. Hu, "On the diversity in the thermal transport properties of graphene: A first-principles-benchmark study testing different exchange-correlation functionals," Comput. Mater. Sci. **151**, 153–159 (2018).
[77]A. Taheri, C. Da Silva, and C. H. Amon, "First-principles phonon thermal transport in graphene: Effects of exchange-correlation and type of pseudopotential," J. Appl. Phys. **123**, 215105 (2018).
[78]M. Arrigoni and G. K. H. Madsen, "Comparing the performance of LDA and GGA functionals in predicting the lattice thermal conductivity of III-V semiconductor materials in the zincblende structure: The cases of AlAs and BAs," Comput. Mater. Sci. **156**, 354–360 (2019).
[79]J. Wei, Z. Xia, Y. Xia, and J. He, "Hierarchy of exchange-correlation functionals in computing lattice thermal conductivities of rocksalt and zinc-blende semiconductors," Phys. Rev. B **110**, 035205 (2024).
[80]Z. Chang, K. Yuan, J. Li, Z. Sun, J. Zheng, M. Al-Fahdi, Y. Gao, B. Wei, X. Zhang, M. Hu *et al.*, "Anomalous thermal conductivity induced by high dispersive optical phonons in rubidium and cesium halides," ES Energy Environ. **16**, 30–39 (2022).
[81]W. Li and N. Mingo, "Thermal conductivity of bulk and nanowire InAs, AlN, and BeO polymorphs from first principles," J. Appl. Phys. **114**, 183505 (2013).
[82]N. Shulumba, Z. Raza, O. Hellman, E. Janzén, I. A. Abrikosov, and M. Odén, "Impact of anharmonic effects on the phase stability, thermal transport, and electronic properties of AlN," Phys. Rev. B **94**, 104305 (2016).
[83]Y. Wang, A. Liu, X. Yang, and X. Zhou, "Anomalous thermal conductivity anisotropy in bulk hexagonal AlN induced by structural phase transition," Appl. Phys. Lett. **126**, 202207 (2025).

[84]S. Baroni, S. de Gironcoli, A. Dal Corso, and P. Giannozzi, "Phonons and related crystal properties from density-functional perturbation theory," Rev. Mod. Phys. **73**, 515–562 (2001).
[85]X. Zhang, C. Shao, and H. Bao, "Cryogenic thermal transport properties from accelerated first-principles calculations: Role of boundary and isotope scattering," Phys. Rev. B **110**, 224301 (2024).
[86]Z. Li, Y. Xia, and C. Wolverton, "First-principles calculations of lattice thermal conductivity in Tl_3VSe_4: Uncertainties from different approaches of force constants," Phys. Rev. B **108**, 184307 (2023).
[87]H. Zhou, S. Zhou, Z. Hua, K. Bawane, and T. Feng, "Extreme sensitivity of higher-order interatomic force constants and thermal conductivity to the energy surface roughness of exchange-correlation functionals," Appl. Phys. Lett. **123**, 192201 (2023).
[88]H. Babaei, R. Guo, A. Hashemi, and S. Lee, "Machine-learning-based interatomic potential for phonon transport in perfect crystalline si and crystalline Si with vacancies," Phys. Rev. Mater. **3**, 074603 (2019).
[89]P. Korotaev, I. Novoselov, A. Yanilkin, and A. Shapeev, "Accessing thermal conductivity of complex compounds by machine learning interatomic potentials," Phys. Rev. B **100**, 144308 (2019).
[90]B. Mortazavi, E. V. Podryabinkin, I. S. Novikov, T. Rabczuk, X. Zhuang, and A. V. Shapeev, "Accelerating first-principles estimation of thermal conductivity by machine-learning interatomic potentials: A MTP/ShengBTE solution," Comput. Phys. Commun. **258**, 107583 (2021).
[91]Z. Liu, X. Yang, B. Zhang, and W. Li, "High thermal conductivity of wurtzite boron arsenide predicted by including four-phonon scattering with machine learning potential," ACS Appl. Mater. Interfaces **13**, 53409–53415 (2021).
[92]B. Póta, P. Ahlawat, G. Csányi, and M. Simoncelli, "Thermal conductivity predictions with foundation atomistic models," arXiv:2408.00755 (2024).
[93]A. Antao, J. D. Burton, D. Dawson, J. Gemmill, Z. Gerstener, B. Godfrey, S. Groel, Z. Jordan, B. Ligon, D. Smith *et al.*, "Modernizing Clemson University's Palmetto Cluster: Lessons learned from 17 years of hpc administration," in *Practice and Experience in Advanced Research Computing 2024: Human Powered Computing* (ACM, 2024), pp. 1–9, available at https://doi.org/10.1145/3626203.3670543.
[94]R. Masuki, T. Nomoto, R. Arita, and T. Tadano, "Ab initio structural optimization at finite temperatures based on anharmonic phonon theory: Application to the structural phase transitions of BaTiO3," Phys. Rev. B **106**, 224104 (2022).